CHAPTER

S9

Atlantic Ocean: Supplementary Materials

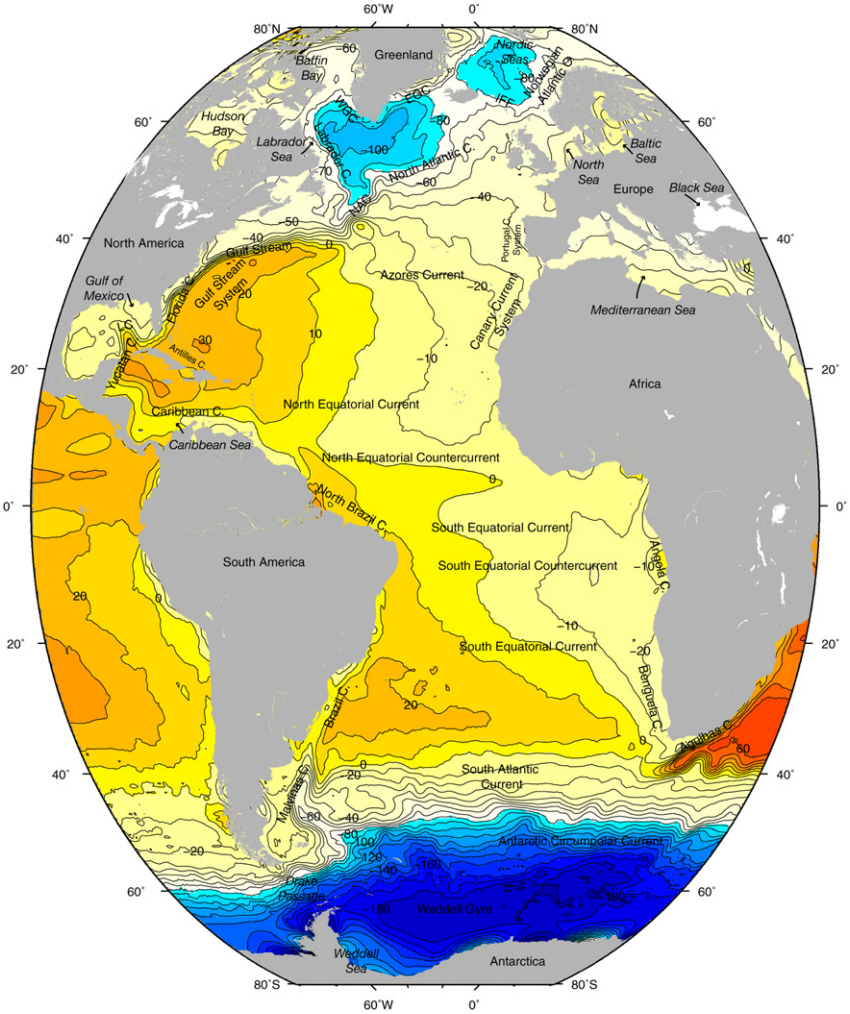

FIGURE S9.1 Atlantic Ocean surface height (cm) and surface current names (Table S9.1). *Data from Niiler, Maximenko, and McWilliams (2003).*

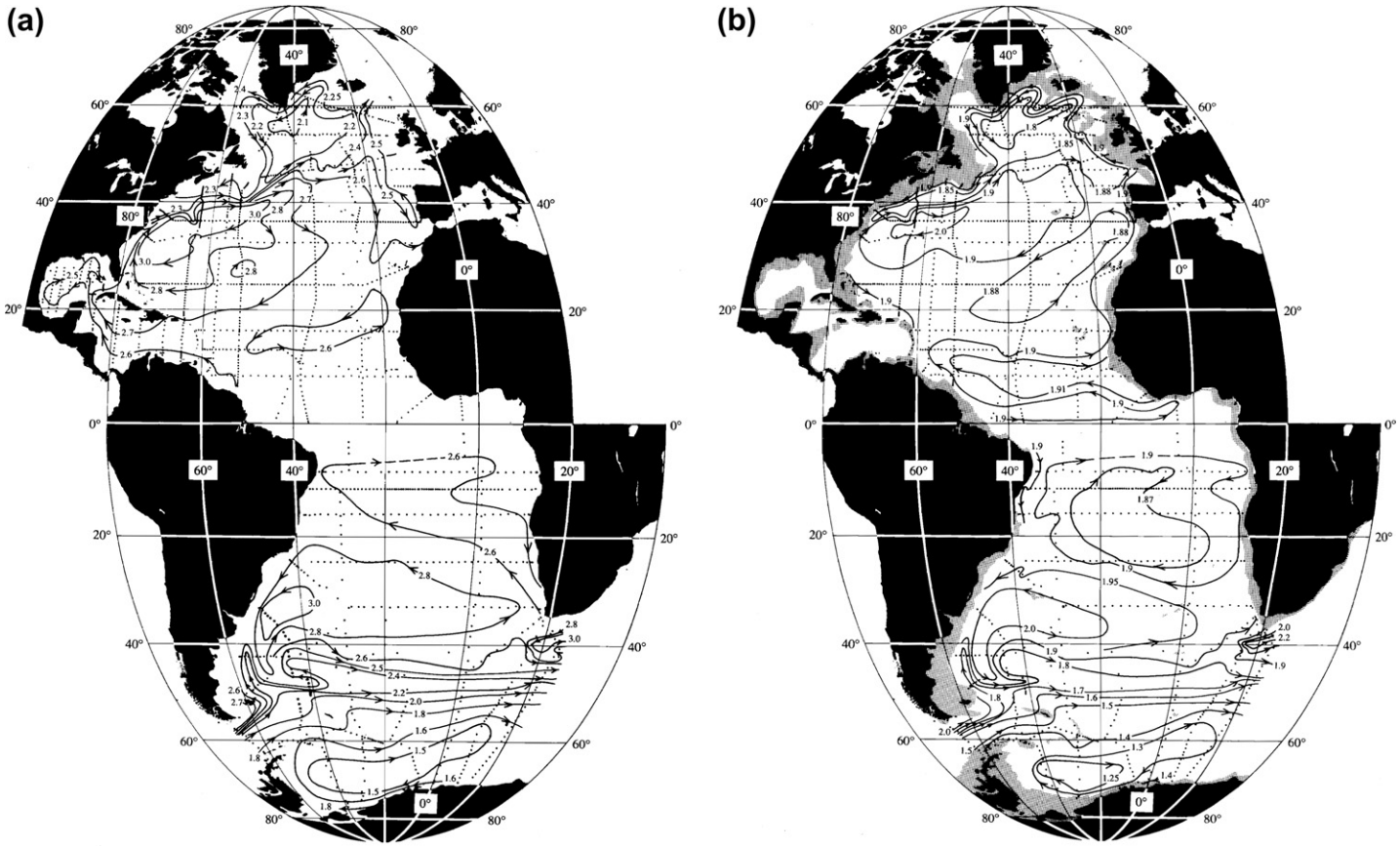

FIGURE S9.2 Geostrophic circulation at (a) 250 dbar, (b) 1000 dbar, and (c) 1500 dbar. The contours are steric height (10 m^2 s^{-2}), adjusted to represent the absolute circulation. *Source: From Reid (1994).*

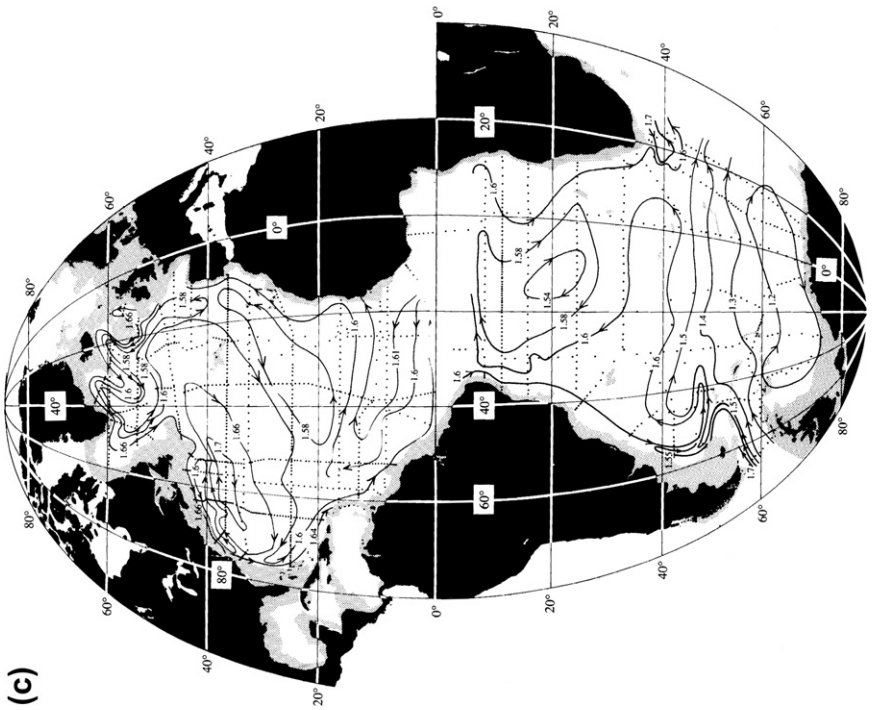

FIGURE S9.2 (*Continued*).

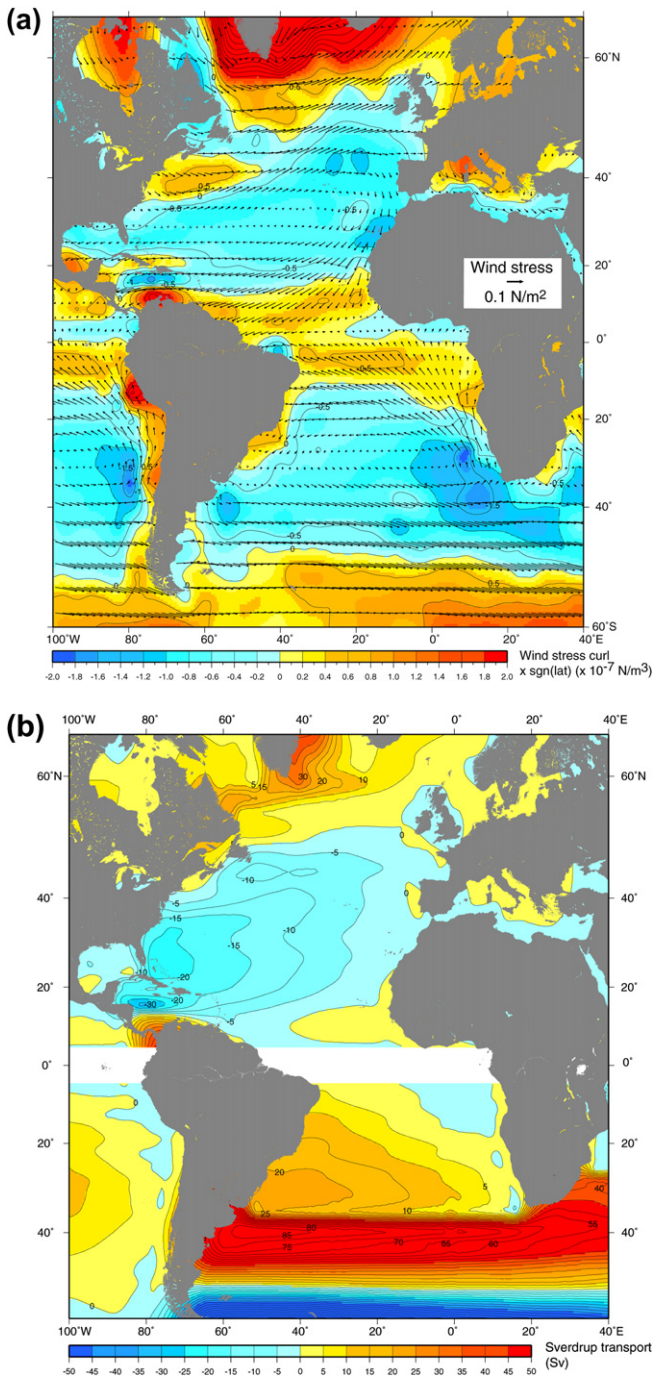

FIGURE S9.3 Annual mean winds. (a) Wind stress (N/m^2) (vectors) and wind-stress curl ($\times 10^{-7}$ N/m^3) (color), multiplied by -1 in the Southern Hemisphere. (b) Sverdrup transport (Sv), where blue is clockwise and yellow-red is counterclockwise circulation. Data are from the NCEP reanalysis 1968–1996 (Kalnay et al., 1996).

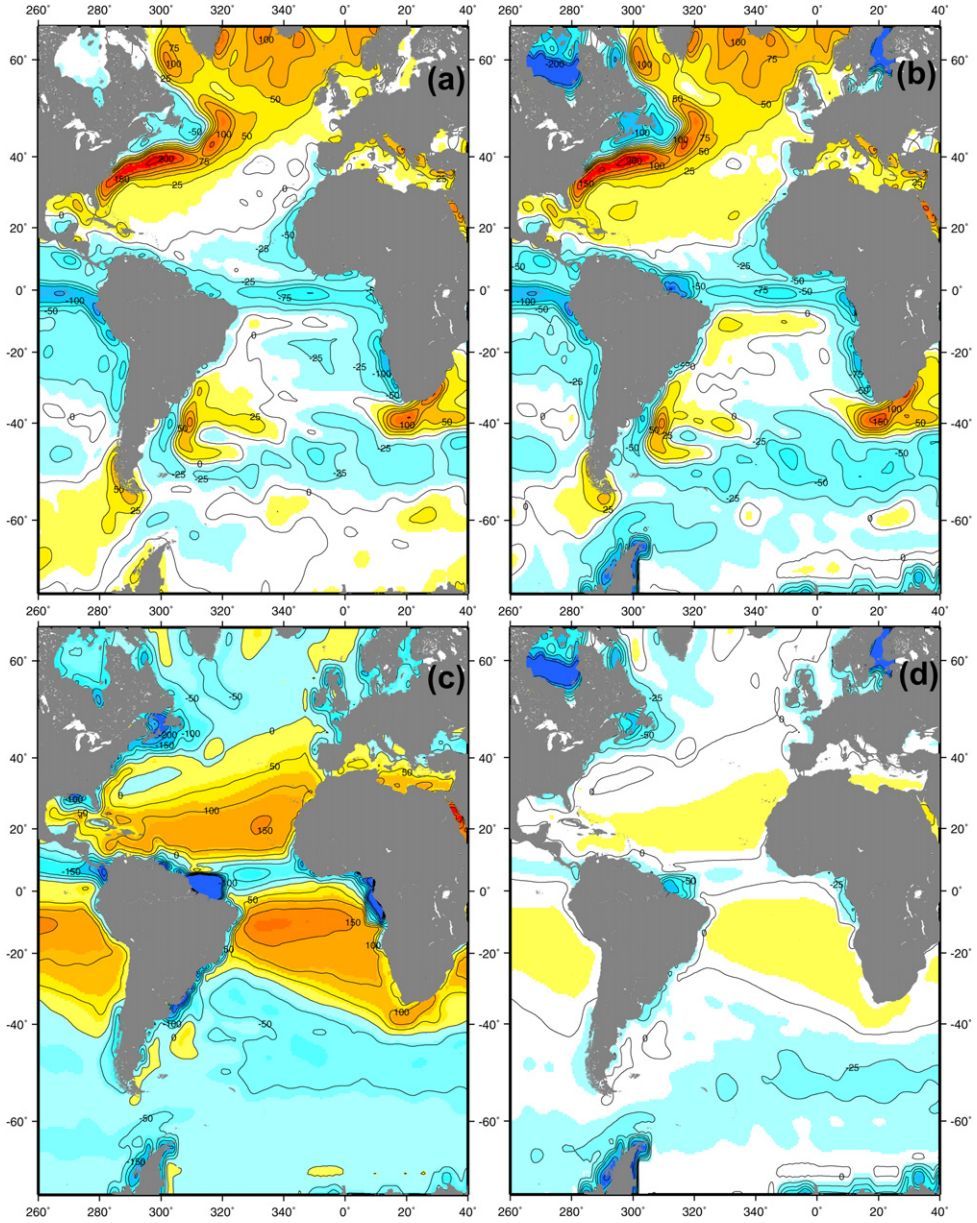

FIGURE S9.4 Annual mean buoyancy forcing, using fluxes for 1997–2006. Data are from Large and Yeager (2009). (a) Net air–sea heat flux (W/m^2). (b) Buoyancy forcing (equivalent W/m^2). (c,d) Net evaporation minus (precipitation + runoff) (cm/yr and equivalent W/m^2). Values less than 10 W/m^2 are white.

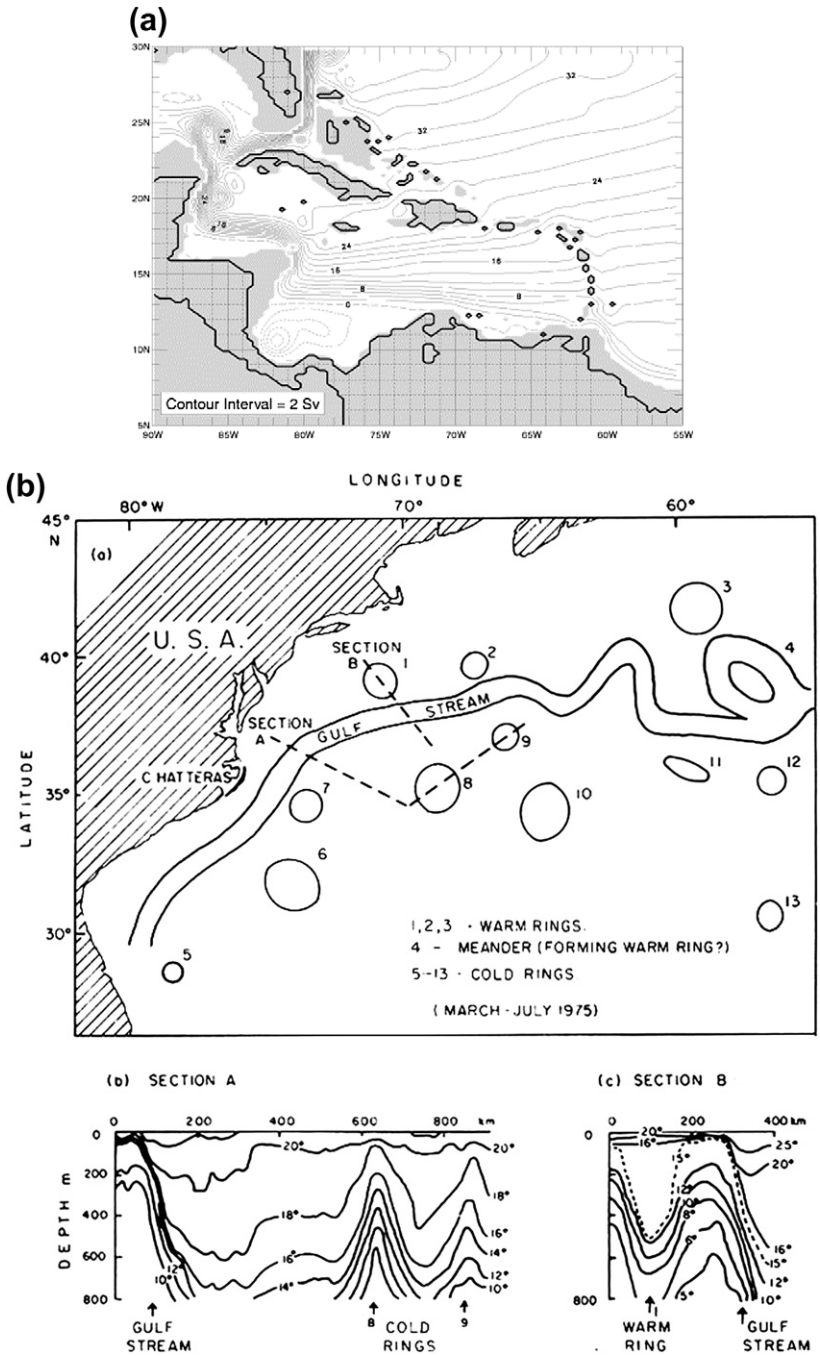

FIGURE S9.5 (a) Modeled transport streamfunction. *Source: From Johns, Townsend, Fratantoni, and Wilson (2002).* (b) Mean velocity from surface drifters (1968–2003); velocities greater than 25 cm/sec are in red. *Source: From Richardson (2005).*

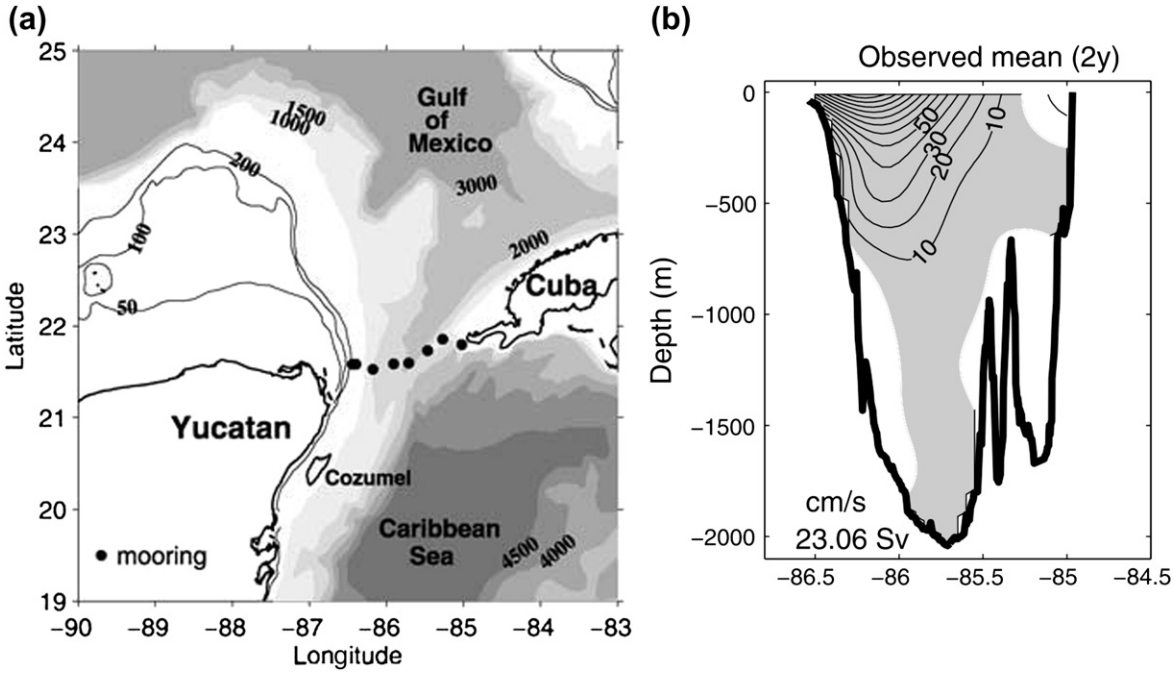

FIGURE S9.6 Flow through Yucatan Channel. (a) Mooring locations for August 1999 to June 2001. (b) Mean northward velocity (cm/sec). Gray is northward flow, white is southward flow. *Source: From Candela et al. (2003).*

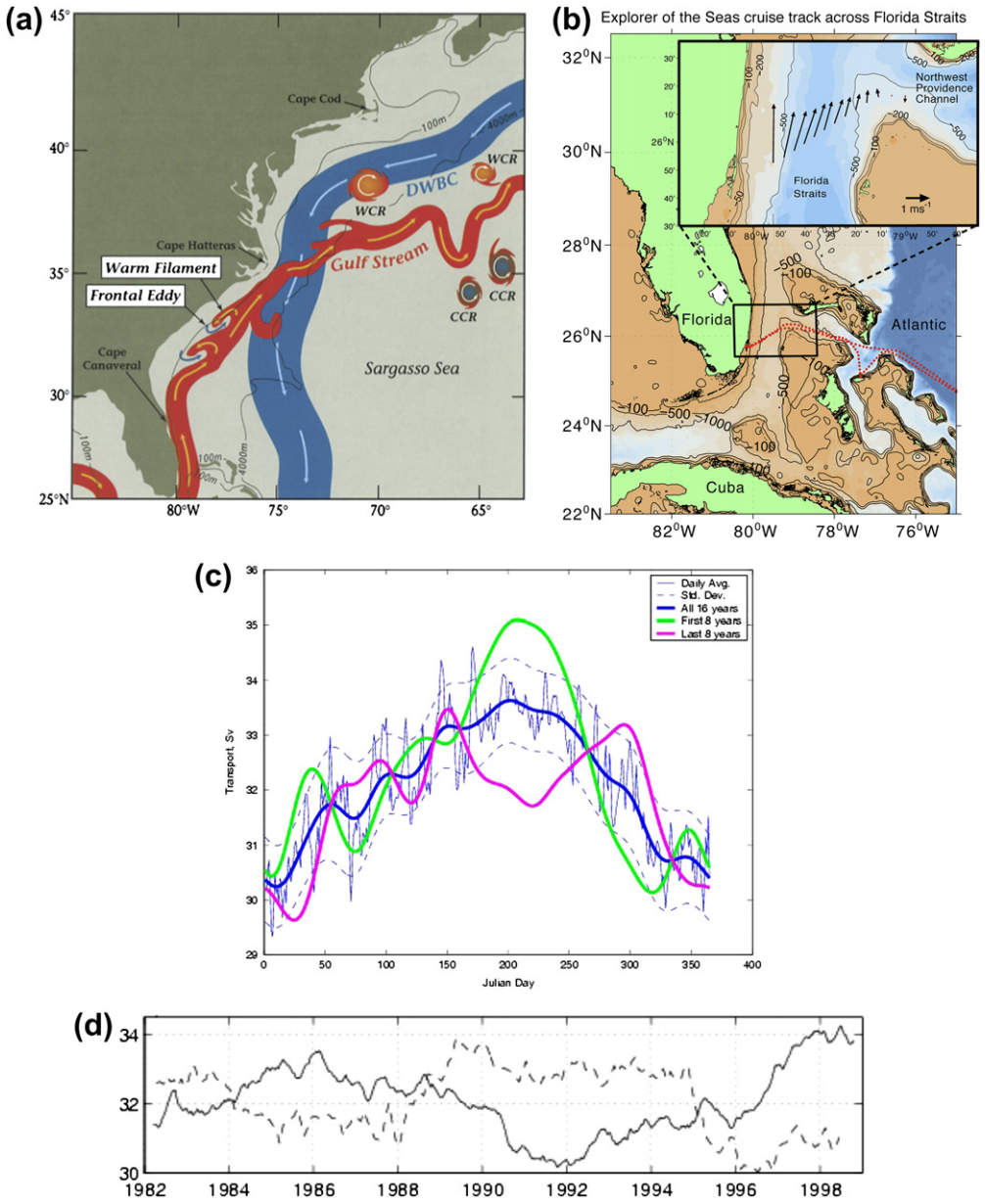

FIGURE S9.7 (a) Florida Current, Gulf Stream, Deep Western Boundary Current, and common eddy features. *Source: From Schmitz (1996), after Bane (1994).* (b) Average 25–75 m velocity from one crossing. *Source: From Beal et al. (2008).* (c) Annual cycle and (d) long-term record of Florida Current transports (solid) with the monthly mean North Atlantic Oscillation index (dashed). *Source: From Baringer and Larsen (2001).*

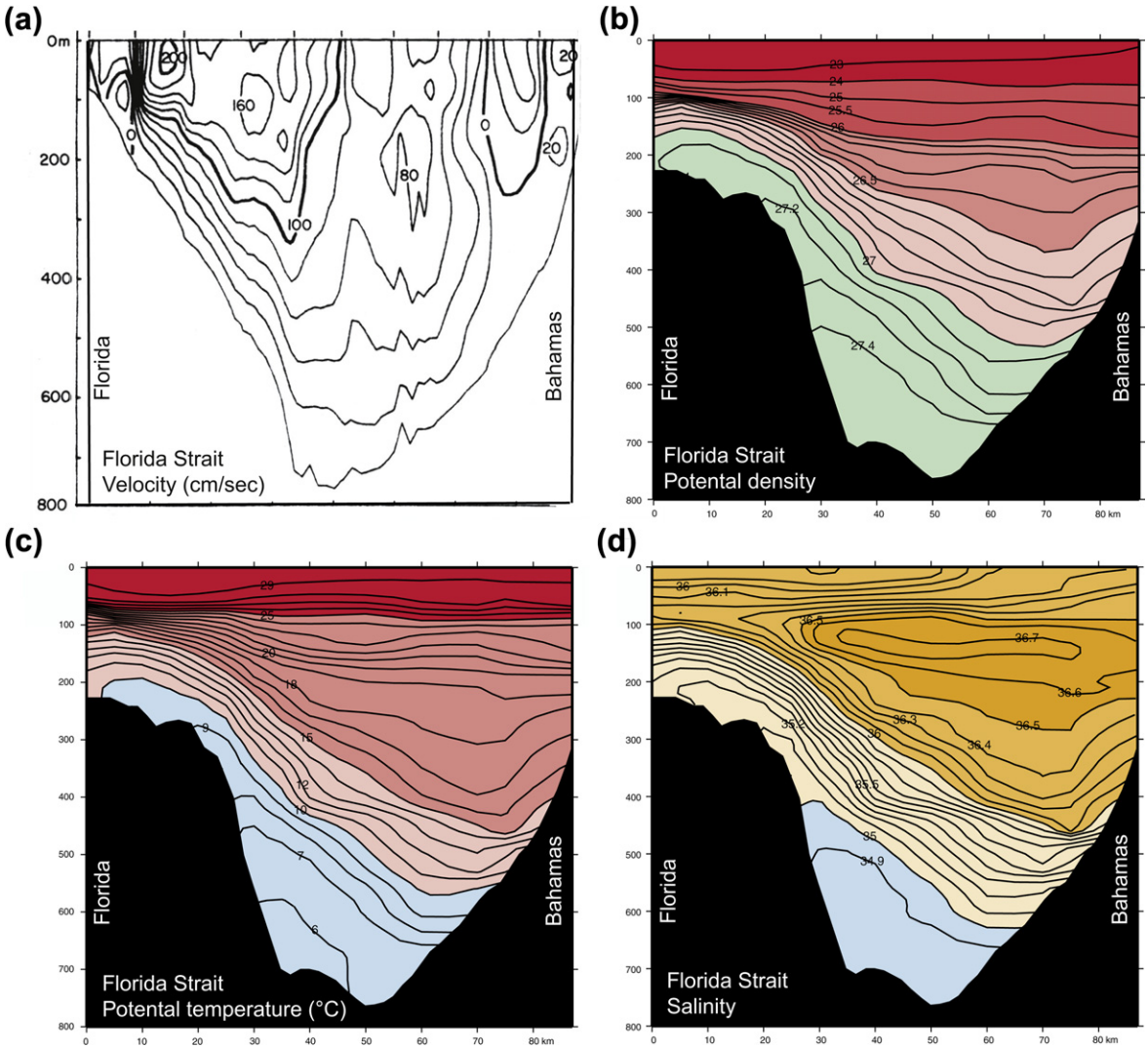

FIGURE S9.8 Florida Strait in September, 1981. (a) Geostrophic velocity (cm/sec). ©American Meteorological Society. Reprinted with permission. *Source: From Roemmich (1983).* (b) Potential density σ_θ (kg/m^3), (c) potential temperature (°C), and (d) salinity.

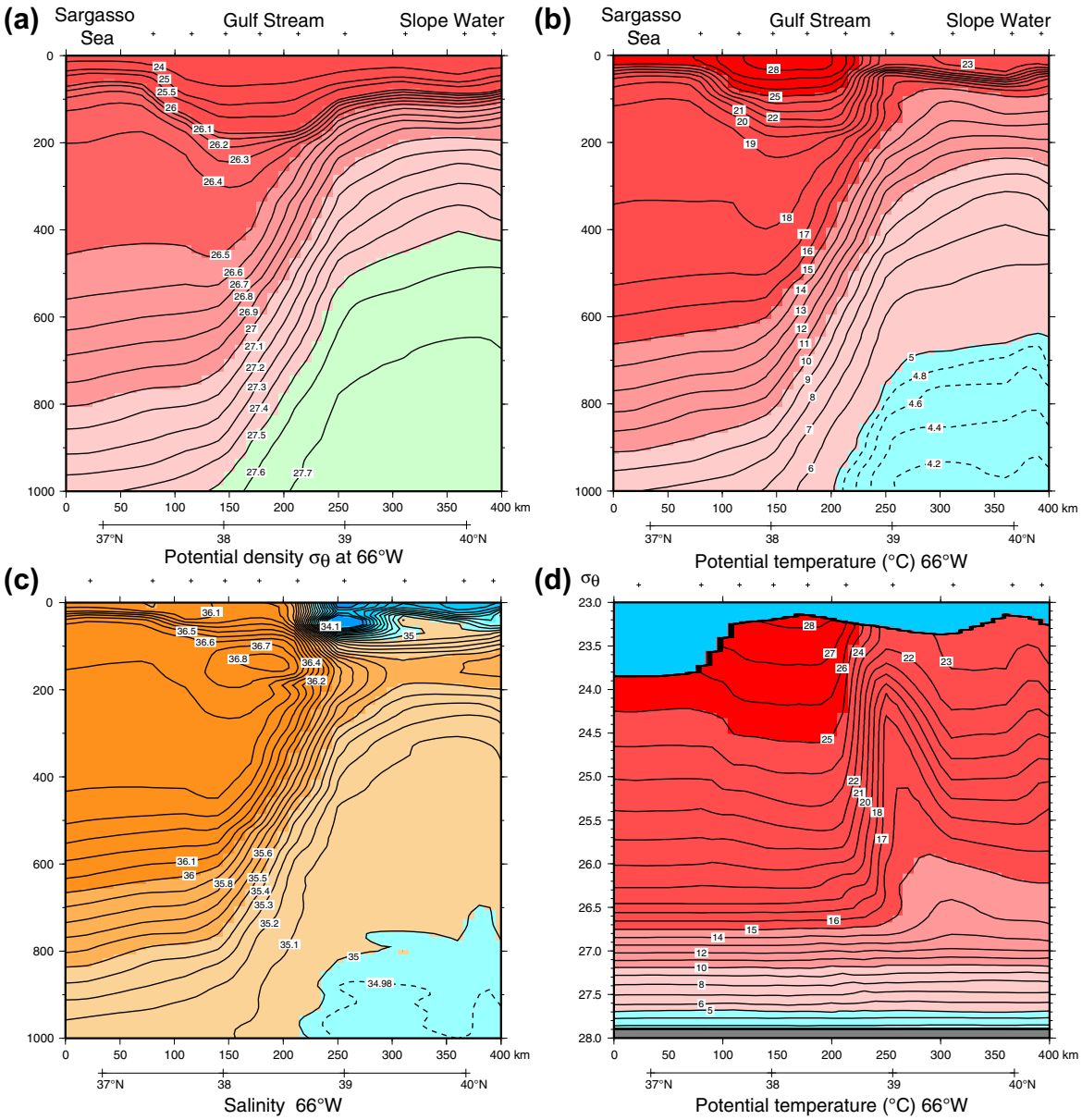

FIGURE S9.9 Gulf Stream properties at 66°W (World Ocean Circulation Experiment section A22 in August, 1997). (a) Potential density σ_θ, (b) potential temperature (°C), (c) salinity, (d) potential temperature with potential density σ_θ as the vertical coordinate.

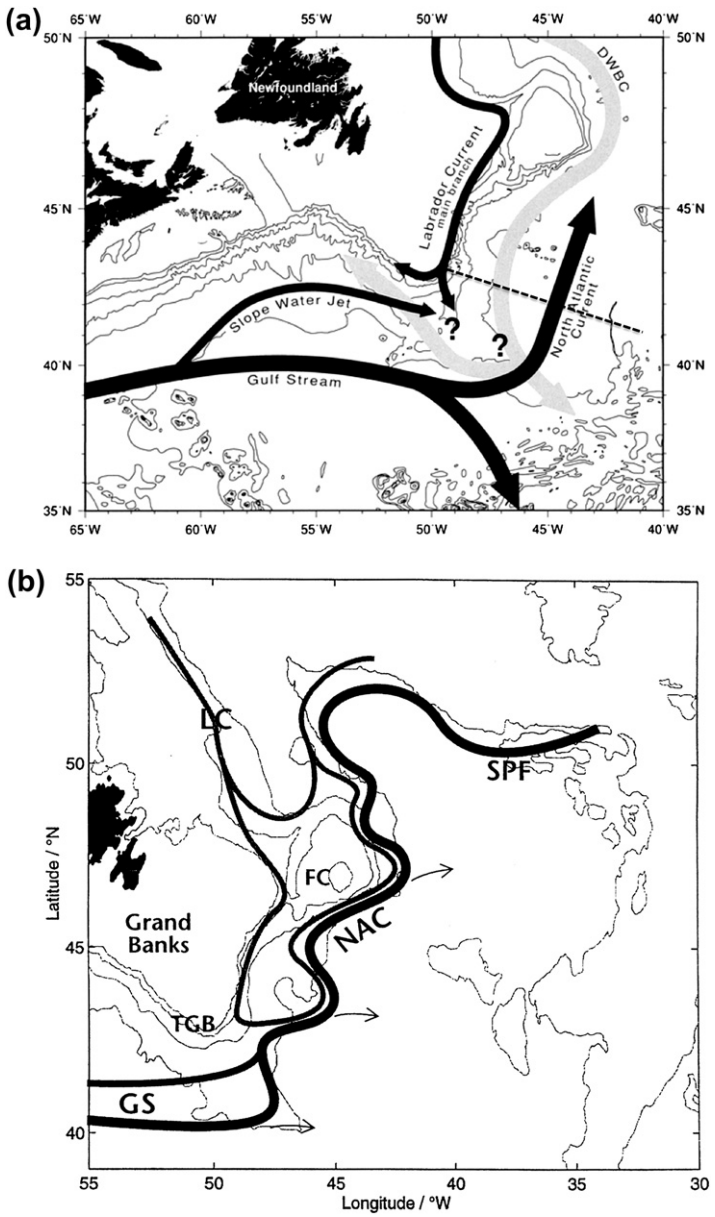

FIGURE S9.10 North Atlantic Current formation region: (a) including the Deep Western Boundary Current (DWBC) ©American Meteorological Society. Reprinted with permission. *Source: From Pickart, McKee, Torres, and Harrington (1999)*, and (b) including eastward detrainments. NAC (North Atlantic Current), GS (Gulf Stream), LC (Labrador Current), SPF (Subpolar Front), FC (Flemish Cap), TGB (Tail of the Grand Banks). *Source: From Rossby (1999).*

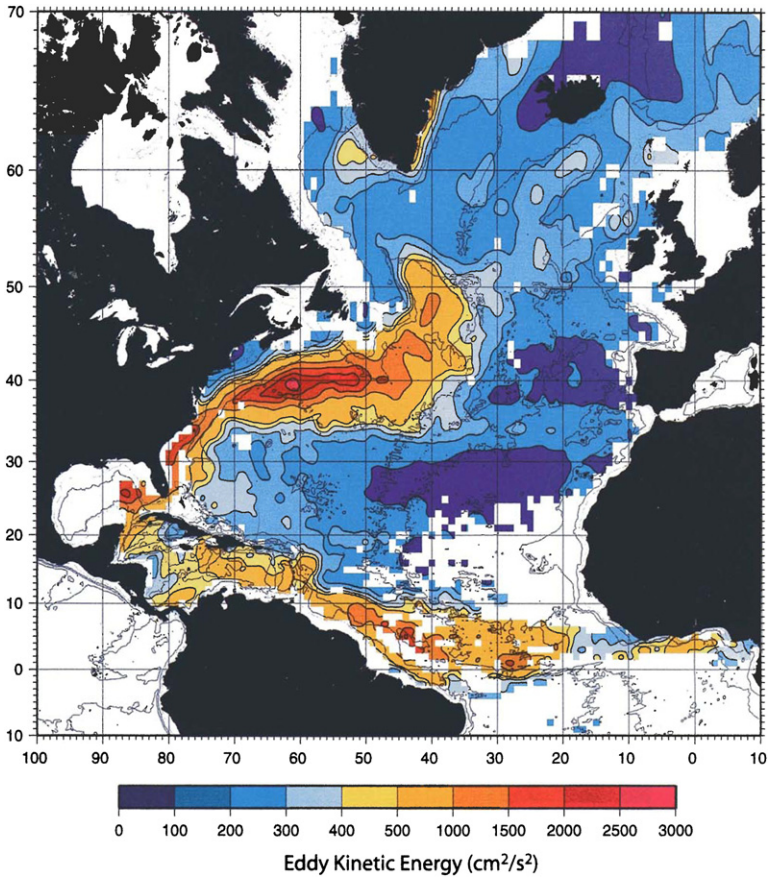

FIGURE S9.11 Eddy kinetic energy of the North Atlantic Ocean (cm^2/s^2) from surface drifter observations from 1990 to 1999. *Source: From Fratantoni (2001).*

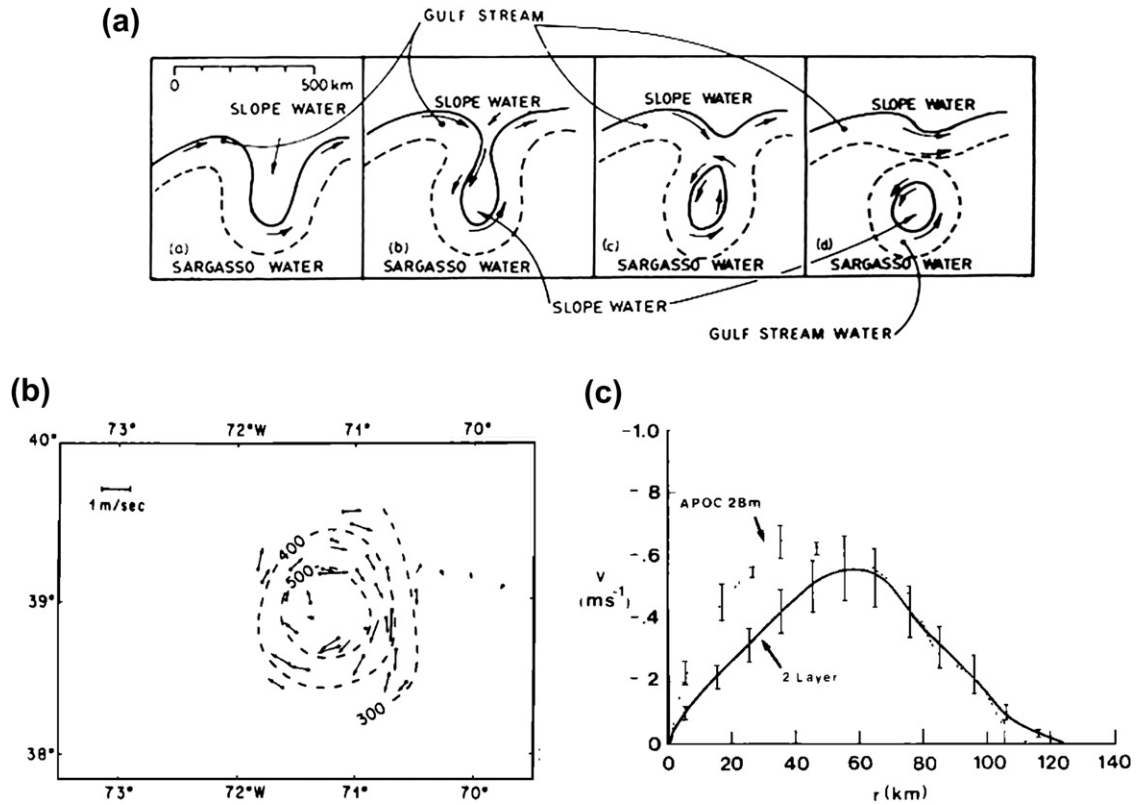

FIGURE S9.12 Gulf Stream rings. (a) Schematic of cold core ring formation from multi-ship observations in Operation Cabot. *After Parker (1971)*. (b,c) Warm core ring observations in April 1982: velocity at 28 m depth and depth of the 10 °C isotherm, and azimuthal velocity near the sea surface (bars) with modeled velocity (solid curve). *Source: From Olson, Schmitt, Kennelly, and Joyce (1985).*

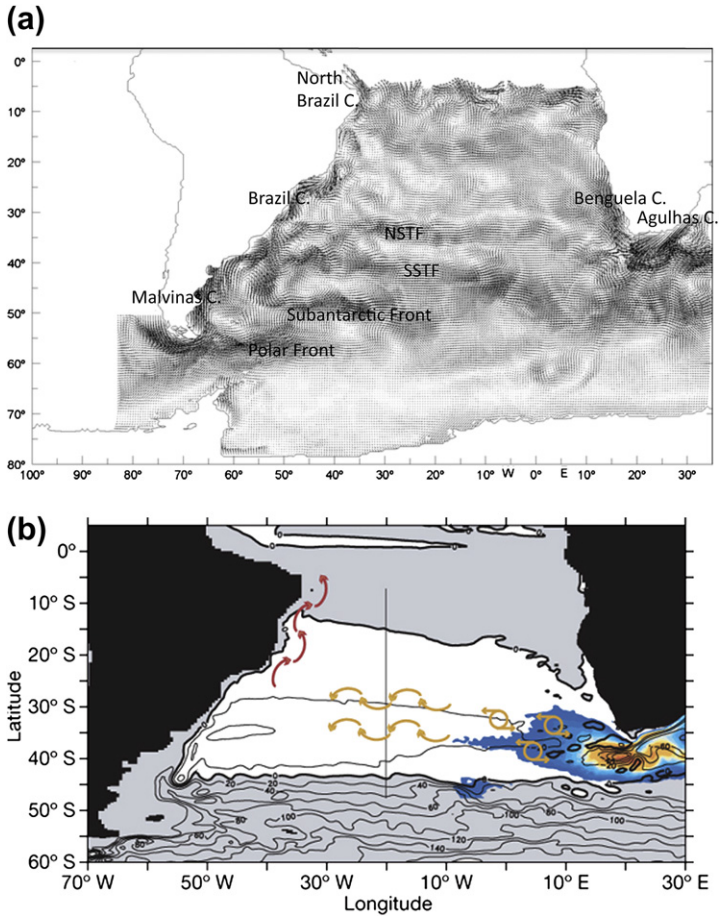

FIGURE S9.13 (a) Surface circulation of the South Atlantic using a temperature/salinity climatology and a β-spiral inverse. ©American Meteorological Society. Reprinted with permission. *Source: From Juliano and Alvés (2007)* with labels added. (b) Streamfunction for the barotropic flow (contours), with pathways of eddies and Rossby waves (yellow) and Kelvin waves (red). Shading is the eddy kinetic energy where it is especially high. *Source: From Biastoch, Böning, and Lutjeharms (2008).*

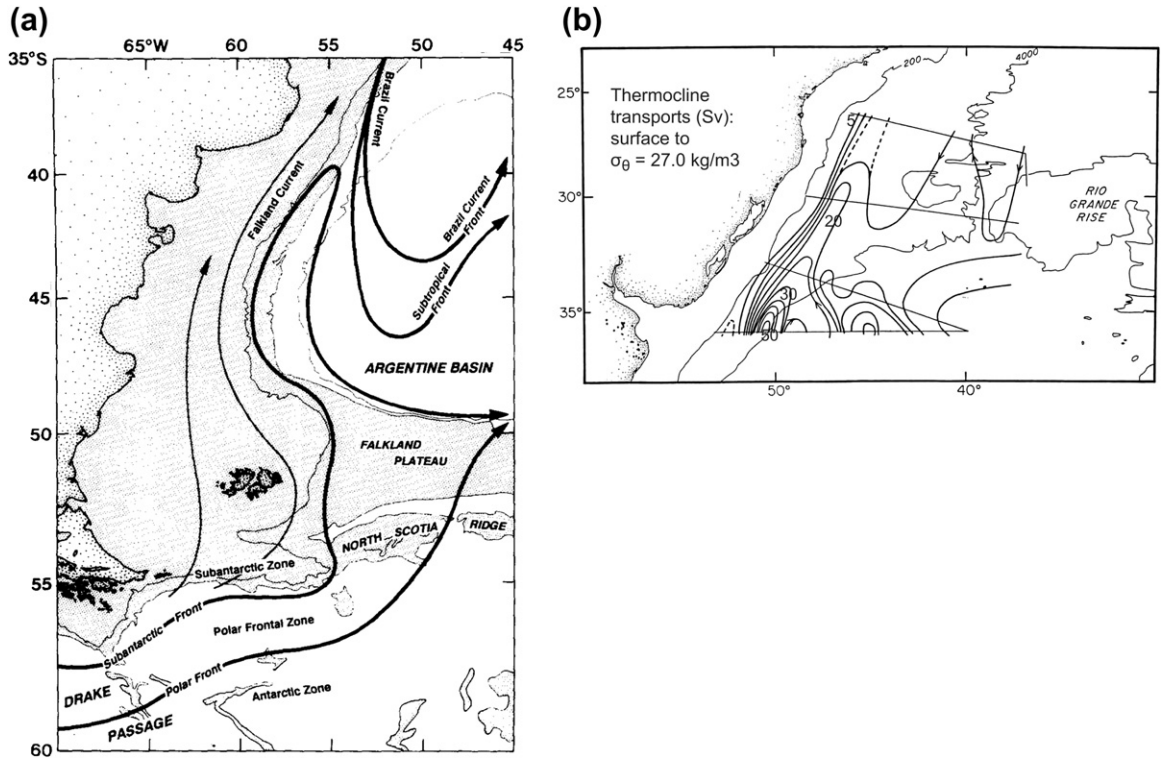

FIGURE S9.14 (a) Schematic of currents and fronts in the confluence region of the Malvinas (Falkland) and Brazil Currents. *Source: From Peterson (1992).* (b) Brazil Current transports, in the thermocline layer (Central Water), based on hydrographic sections (straight lines). Each solid contour is 5 Sv. *After Zemba (1991).* (c) Location and trajectories of warm core Brazil Current rings from 1993 to 1998, superimposed on the rms sea-surface height variability from altimetry data. *Source: From Lentini, Goni, and Olson (2006).*

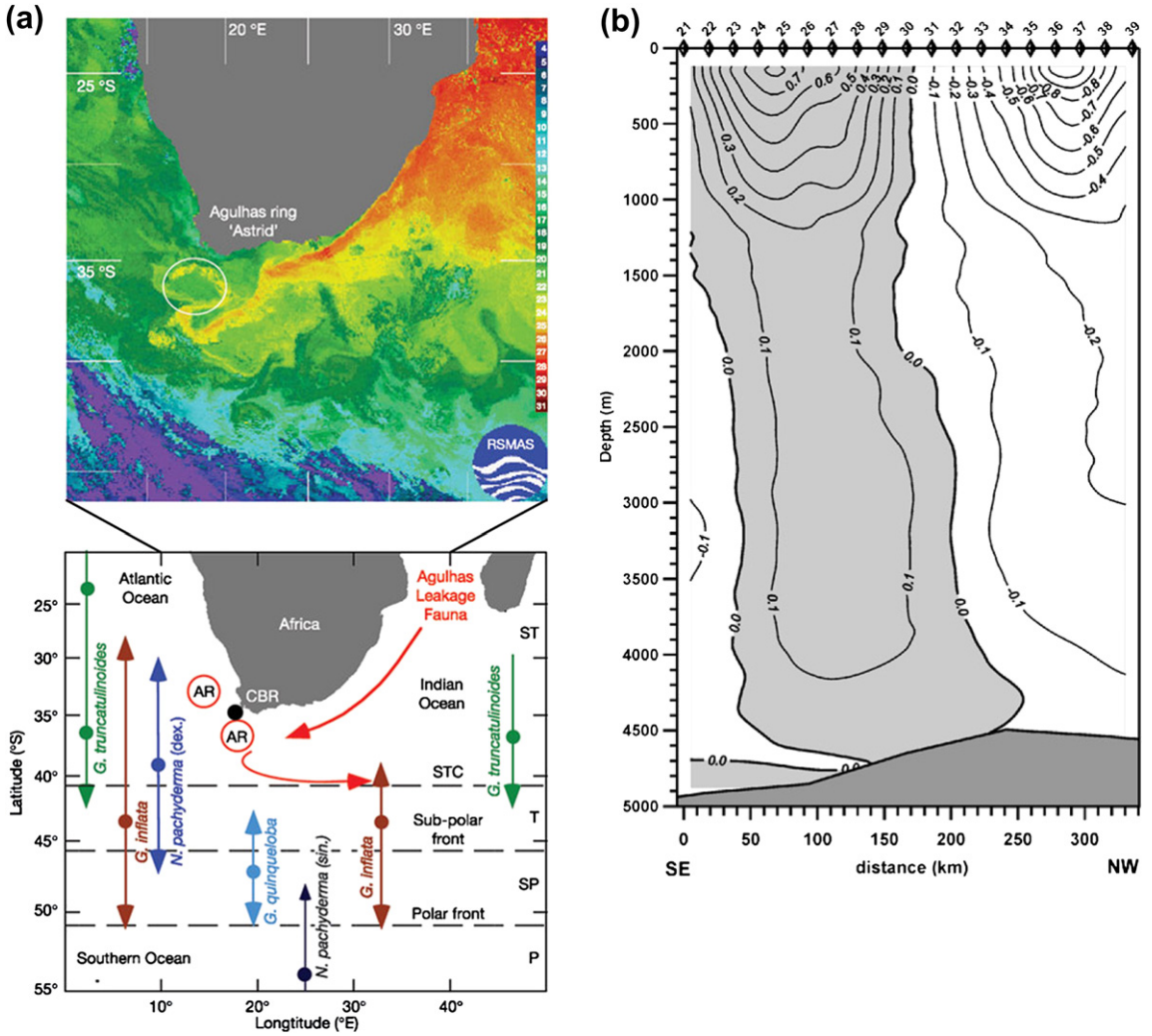

FIGURE S9.15 Agulhas ring "Astrid" in March 2000. (a) SST satellite image. *Source: From Peeters et al. (2004).* (b) Velocity (m/s) from an LADCP, (c) potential temperature, and (d) salinity. *Source: From van Aken et al. (2003).*

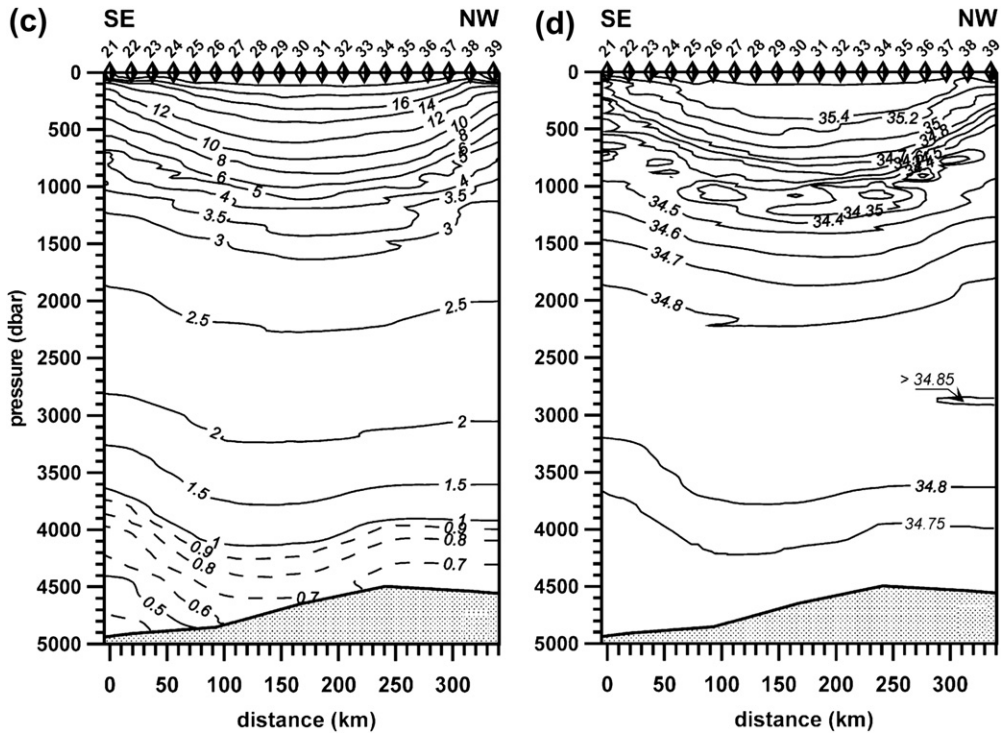

FIGURE S9.15 (*Continued*).

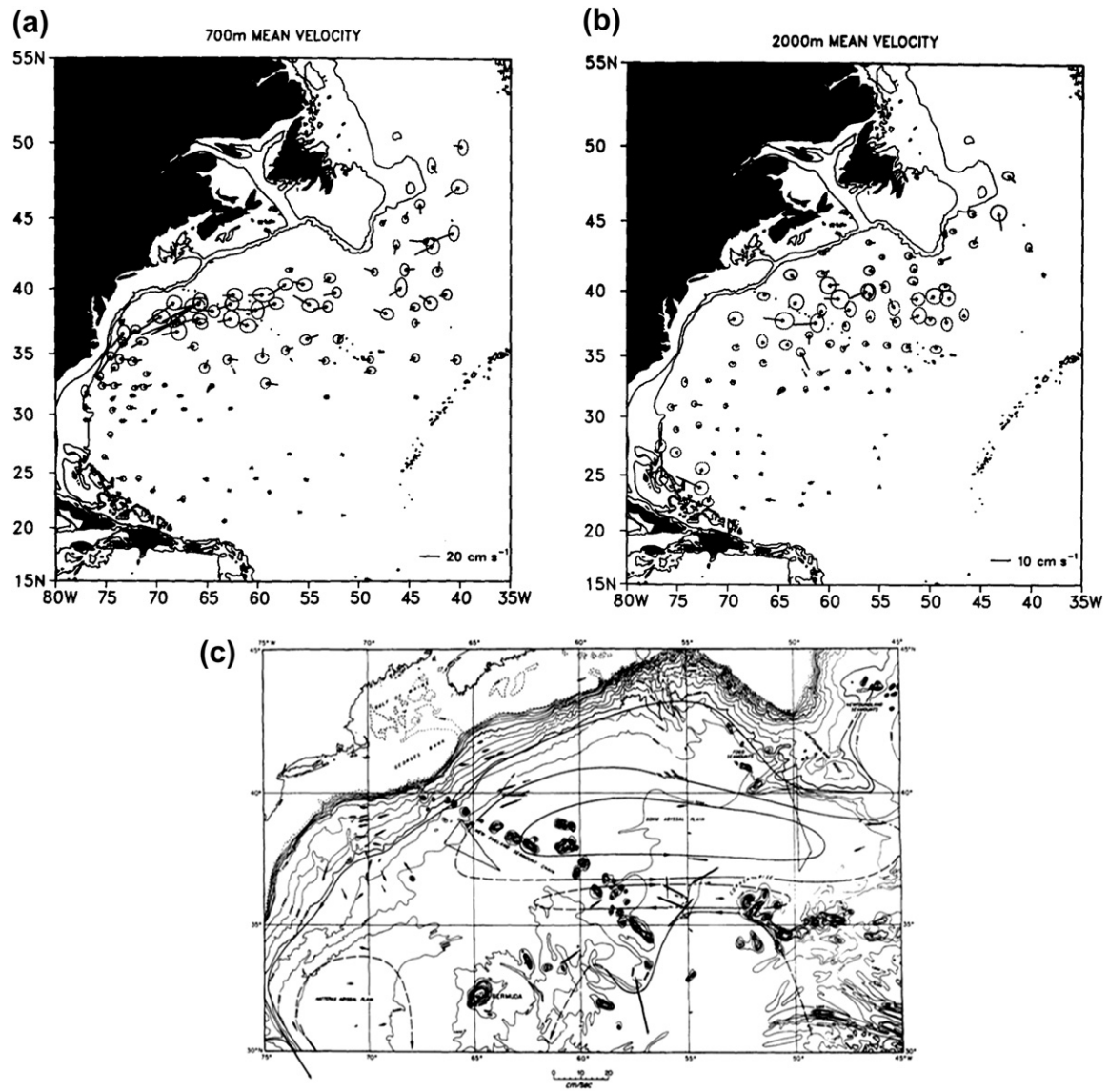

FIGURE S9.16 Deep Gulf Stream structure. (a,b) Mean velocity at 700 and 2000 m, averaged in 1° bins, from acoustically tracked floats. Vectors show mean flow direction and speed; ellipses are the variance. *Source: From Owens (1991).* (c) Mean velocities at 4000 m from current meter observations in the 1970s and suggested streamlines. *Source: From Hogg (1983).*

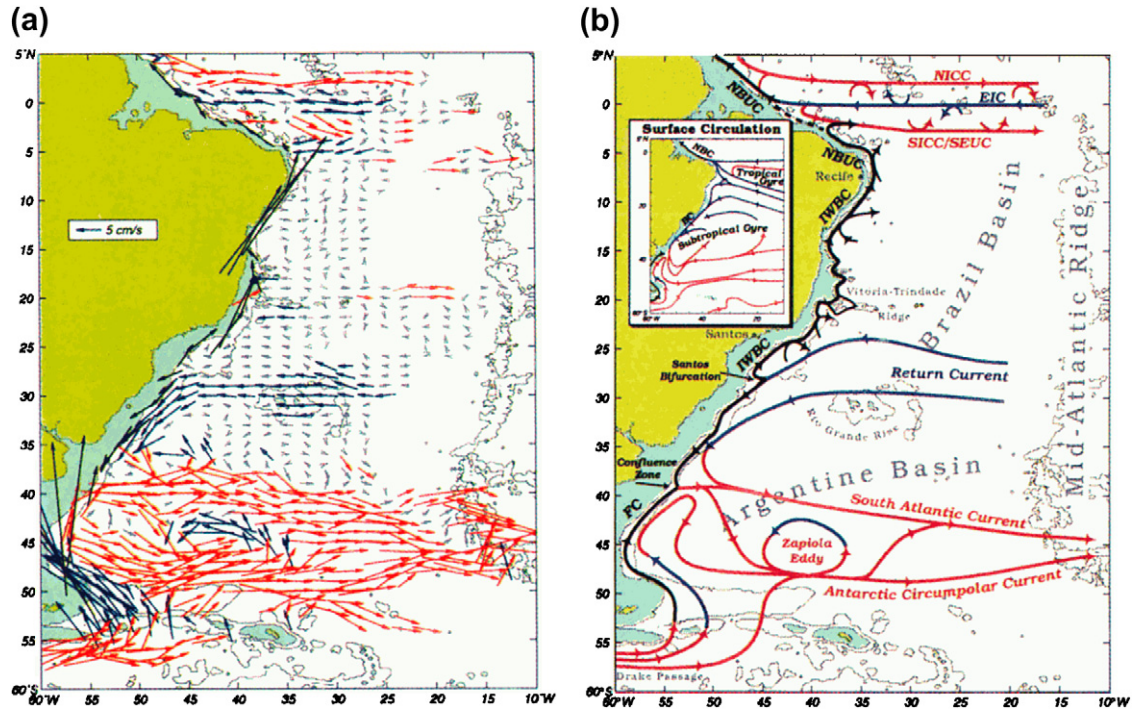

FIGURE S9.17 Deep Brazil and Malvinas Current structure. (a) Mean velocity and (b) circulation schematic at intermediate depth (650–1050 m) based on subsurface floats from different experiments during 1989–1996. *Source: From Boebel et al. (1999).*

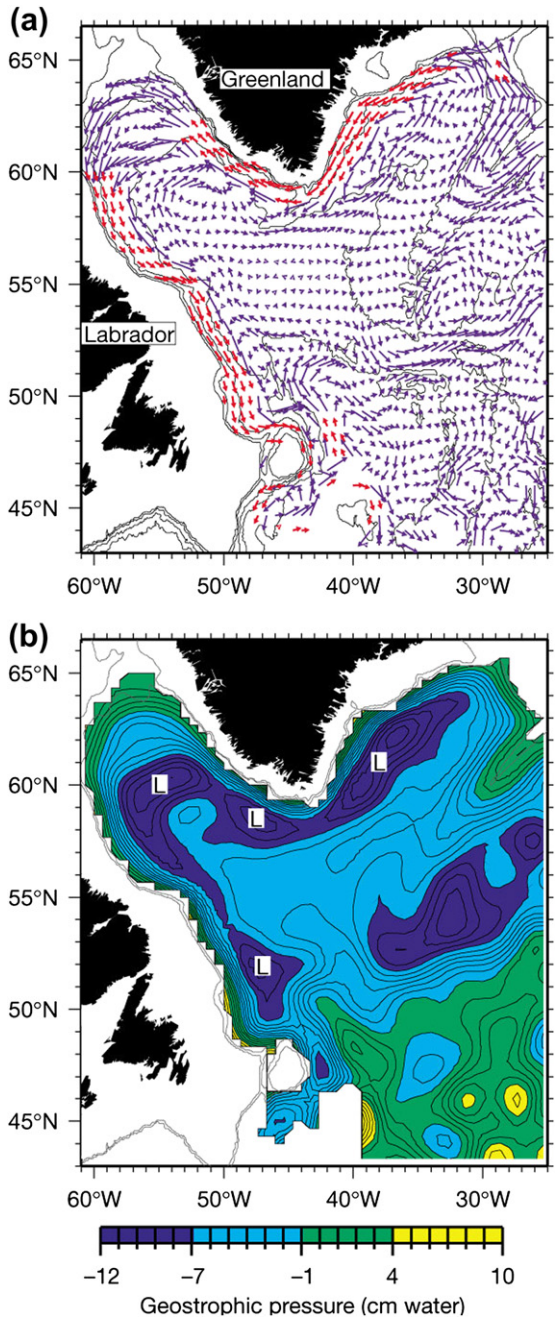

FIGURE S9.18 Mid-depth Labrador Sea circulation. (a) Velocity (cm/sec) and (b) geostrophic pressure (cm) at 700 m from profiling float observations. *Source: From Lavender, Davis, and Owens. (2000).*

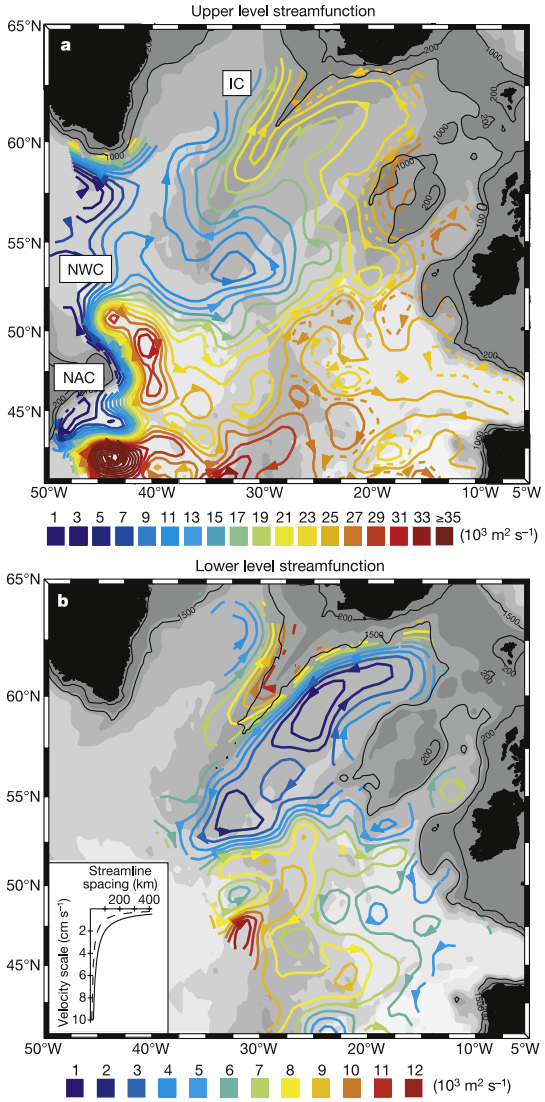

FIGURE S9.19 Mid-depth subpolar circulation. Mean transport streamfunctions on isopycnal $\sigma_\theta = 27.5\ \mathrm{kg/m^3}$, based on acoustically tracked isopycnal floats. *Source: From Bower et al.(2002).*

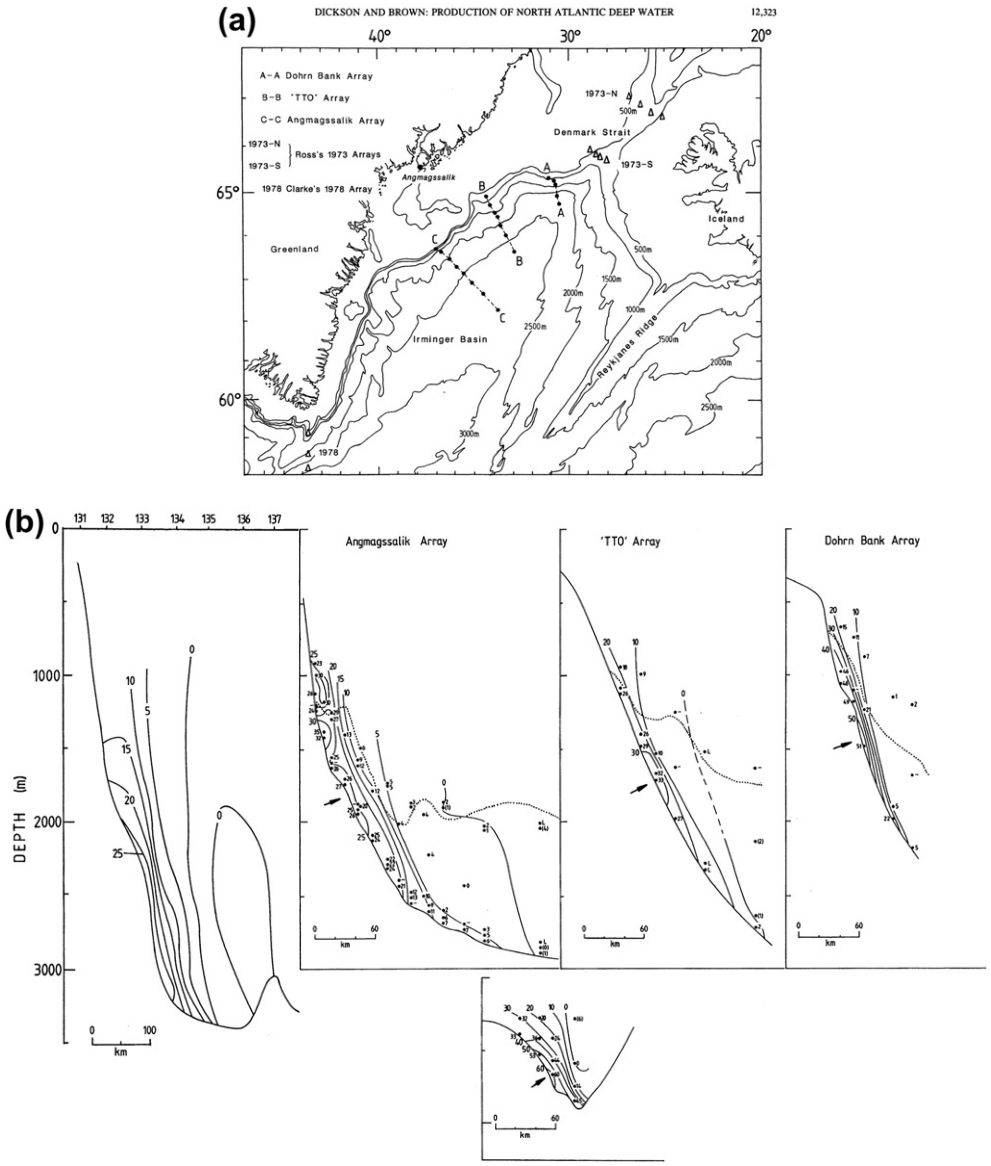

FIGURE S9.20 Mean velocities from current meter deployments in Denmark Strait and along the coast of Greenland from 1986 to 1991. Left to right: Cape Farewell (southern tip of Greenland), 63, 64, and 65°S. Small inset at bottom: just south of the strait. The map shows the location of each line of moorings. *Source: From Dickson and Brown (1994).*

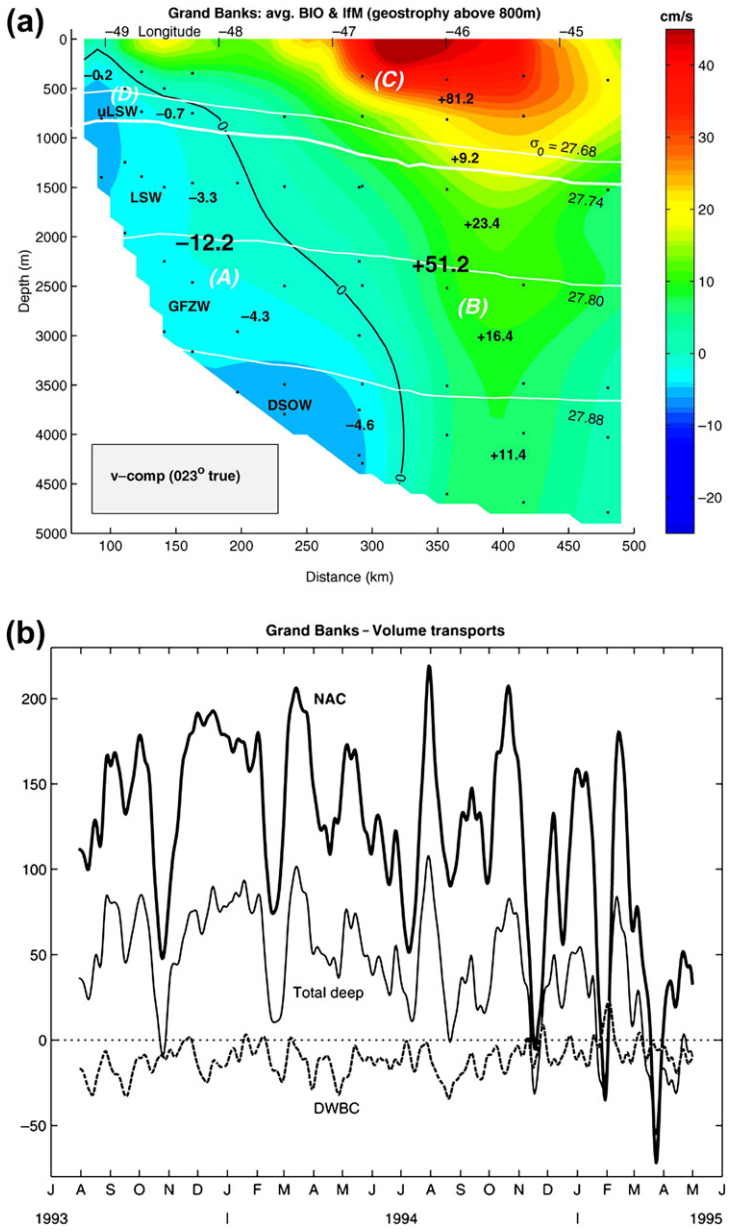

FIGURE S9.21 Deep Western Boundary Current (DWBC) east of the Grand Banks. (a) Mean velocity (color) and transports (numbers in Sv) and (b) transport time series for the DWBC, all deep water and the North Atlantic Current, from current meters at 42°N, 45°W east of the Grand Banks (location in Figure 9.44). Acronyms: LSW, Labrador Sea Water; uLSW, upper LSW; DSOW, Denmark Strait Overflow Water; and GFZW, Gibbs Fracture Zone Water, which is called Northeast Atlantic Deep Water or Iceland Scotland Overflow Water by others. *Source: From Schott et al. (2004).*

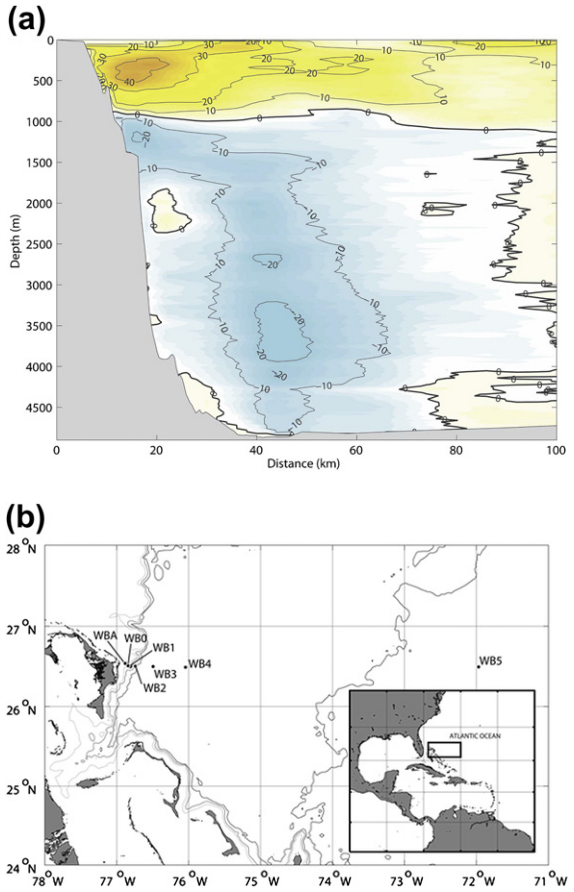

FIGURE S9.22 DWBC east of Florida. (a) DWBC and Antilles Current mean velocity section (Lowered ADCP observations) and (b) location of Abaco moorings (26.5°N). ©American Meteorological Society. Reprinted with permission. *Source: From Johns et al. (2008).*

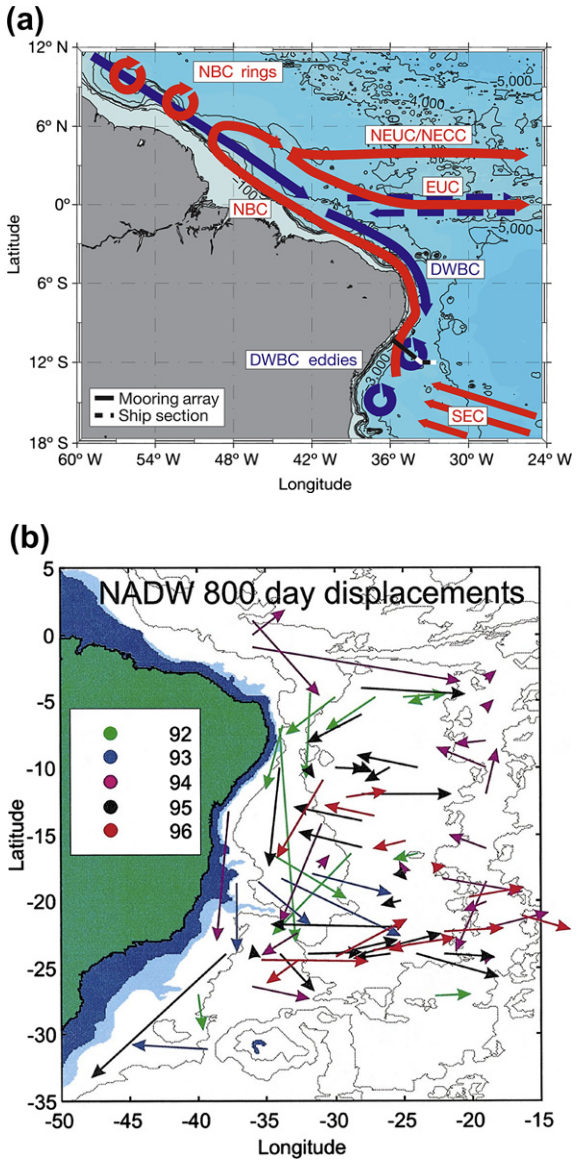

FIGURE S9.23 DWBC east of Brazil. (a) Schematic of the DWBC (blue) and its breakup into eddies south of 8°S. Acronyms for currents are as in Table S9.3. *Source: From Dengler et al. (2004)*. (b) NADW (2500 m) flows in the Brazil Basin based on acoustically tracked floats: float displacements over 800 days. *Source: From Hogg and Owens (1999)*. (c) Mean velocities at current meters at the 30°S moored array across Vema and Hunter Channels. Shaded regions are northward flow. ©American Meteorological Society. Reprinted with permission. *Source: From Hogg, Siedler, & Zenk (1999).*

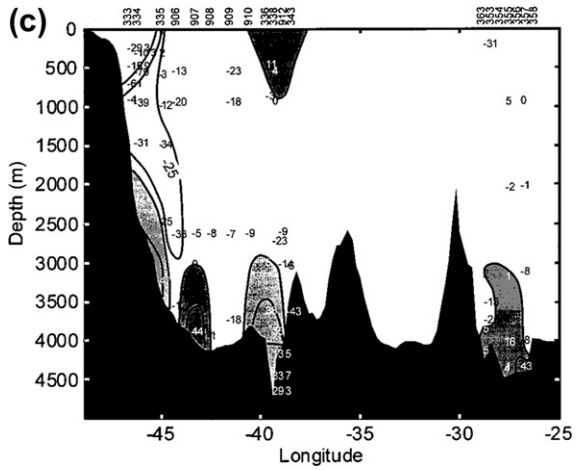

FIGURE S9.23 (*Continued*).

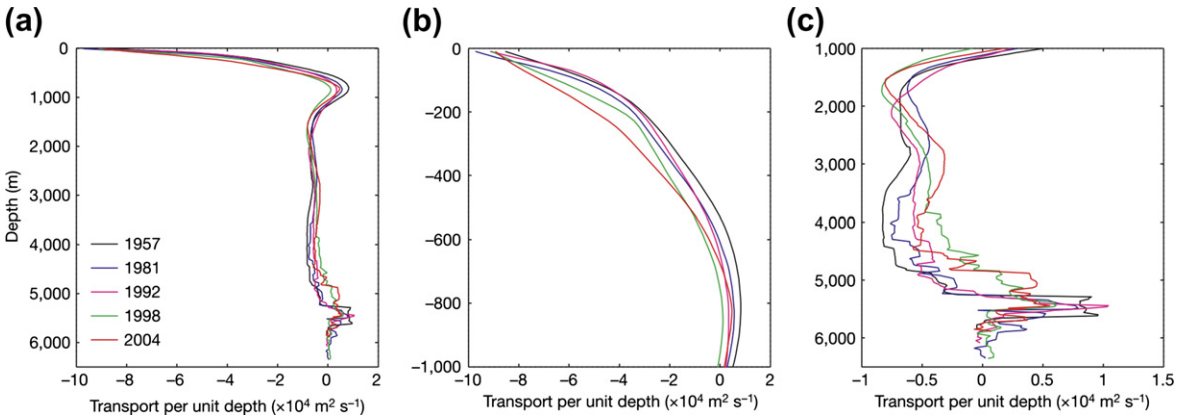

FIGURE S9.24 Meridional transport (geostrophic velocity) at 24–26.5°N in the North Atlantic for five different years. (a) Full depth, (b) 0 to 1000 m, and (c) 1000 m to bottom. *Source: From Bryden, Longworth, and Cunningham (2005b).*

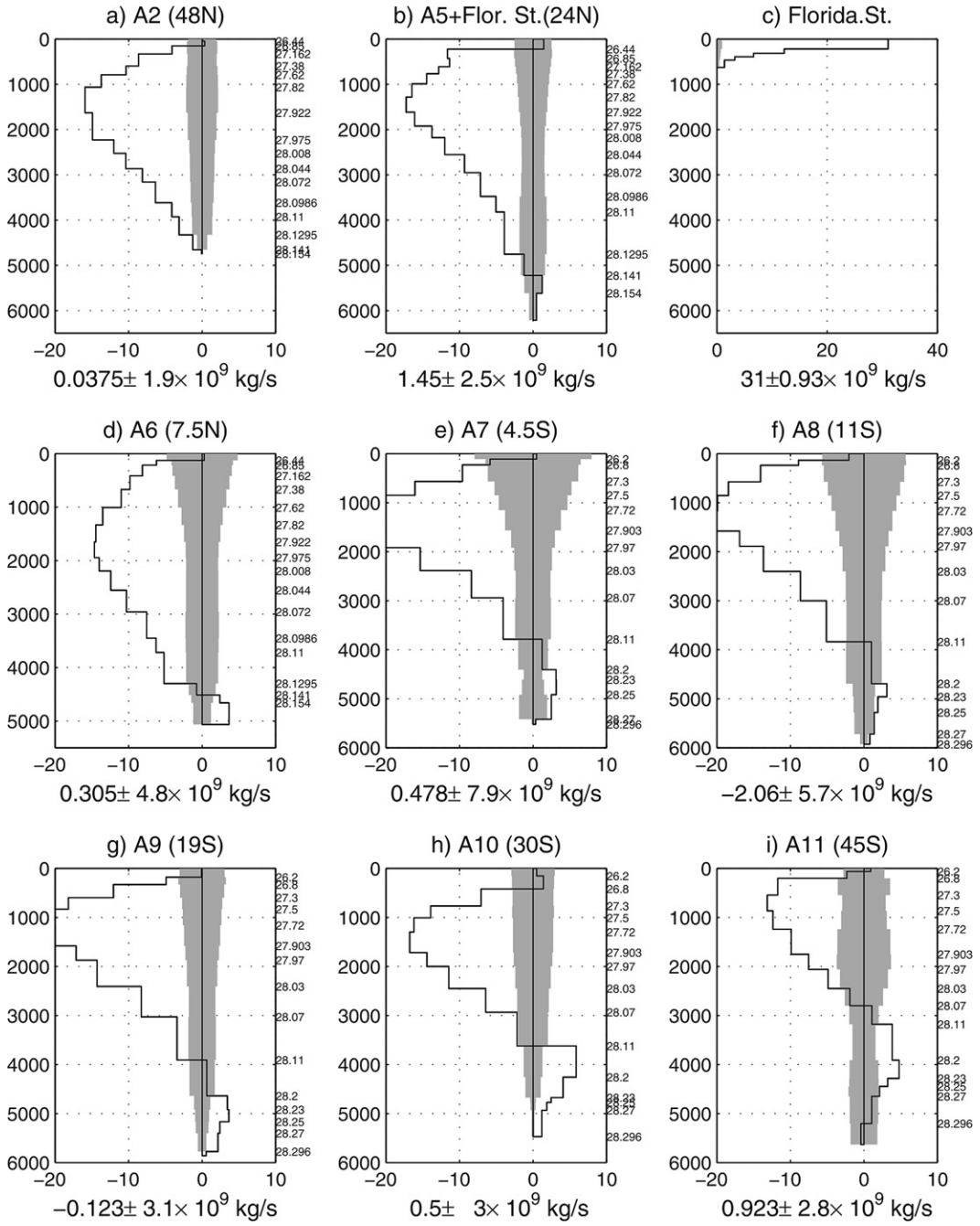

FIGURE S9.25 Northward transports (Sv) across zonal sections in isopycnal layers, integrated upward from zero at the bottom. Section latitudes are indicated in parentheses. Ekman transport is not included. Gray indicates the uncertainty. *Source: From Ganachaud (2003).*

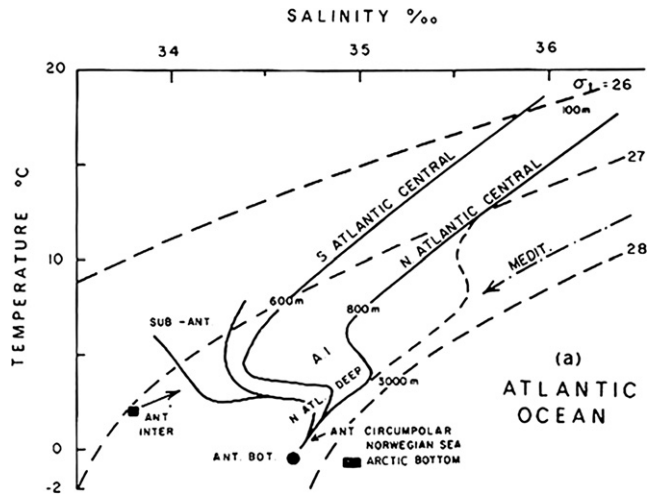

FIGURE S9.26 Schematic temperature — salinity diagram for the main water masses of the Atlantic Ocean.

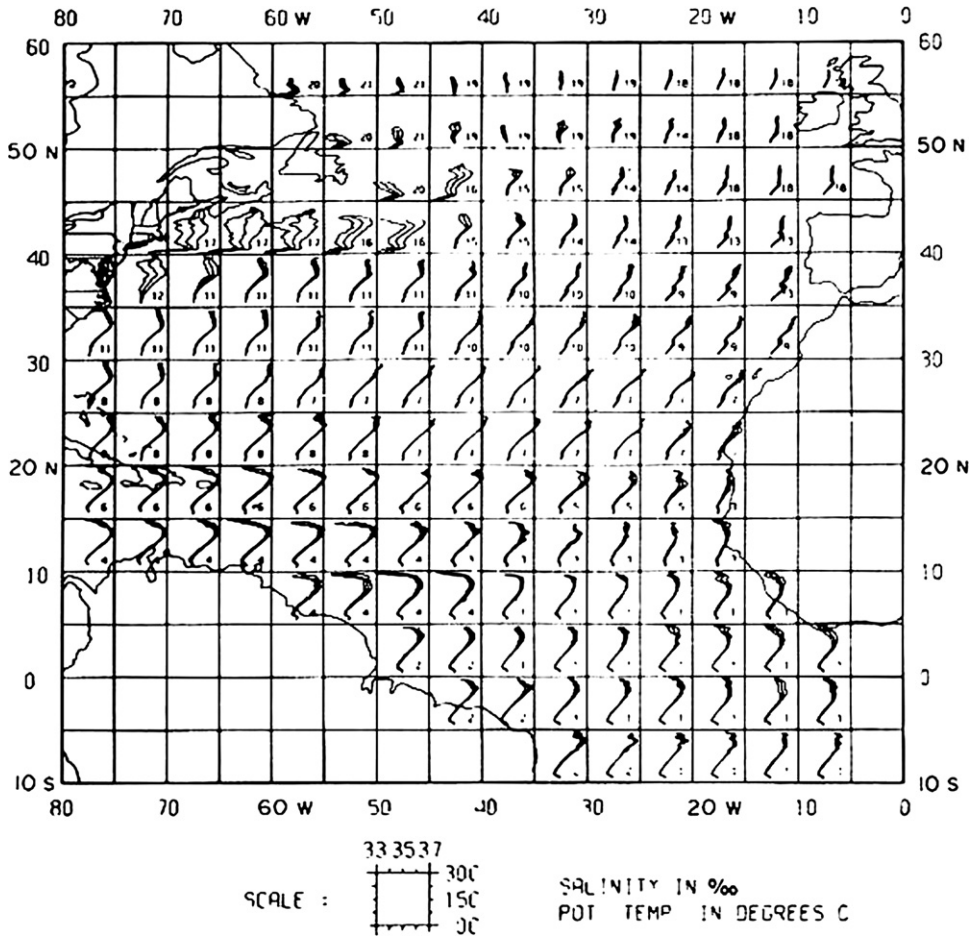

FIGURE S9.27 Atlantic Ocean: mean T-S curves and one standard deviation curves by 5° squares. Extended caption: The largest variability (large standard deviation) is at 40–50 °N off the east coast of North America, due to the Gulf Stream and North Atlantic Current, which each separate strongly contrasting water masses (fresh, cold on the north/west side and saltier, warmer on the south/east side). At 4–6 °C the salinity minimum of the AAIW is well marked in the tropics. It erodes to the north, losing its character by about 20°N. The North Atlantic Central Water connects the AAIW to the high salinity near-surface or surface waters. The STUW (near-surface salinity maximum) is present throughout the tropics south of 20°N. Salinity is highest at the sea surface in the central subtropical gyre; this is the surface source region of the subducted STUW to the south. The Gulf Stream system also has a near-surface salinity maximum, due to northward advection of STUW and saline Central Water, which is overrun by fresher slope water. At mid-latitudes, off the Strait of Gibraltar, the saline outflow from the Mediterranean leads to the salinity maximum of the Mediterranean Water at mid-depth at about 10°C. From the sharp bend in the T-S curves this maximum can be traced as it spreads north, west, and south. In northern latitudes, all temperatures are below 15°C. In the Labrador Sea, the upper ocean waters are colder (and fresher) than the underlying salinity maximum of the NEADW and NSOW. In contrast, the waters in the central far North Atlantic appear almost isohaline over the entire temperature range.

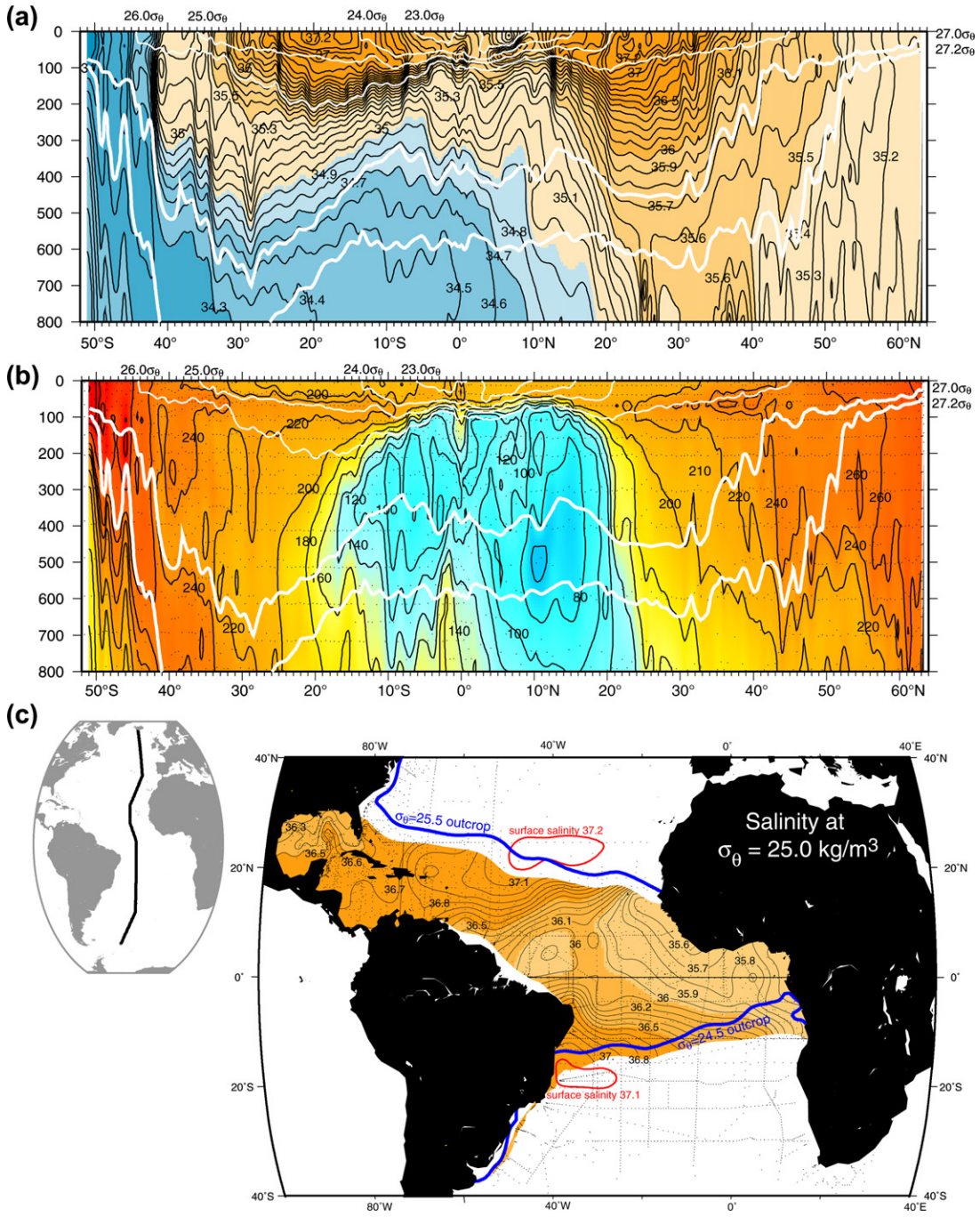

FIGURE S9.28 Subtropical Underwater. Vertical sections of (a) salinity and (b) oxygen (μmol/kg) with selected potential density contours, along approximately 25°W in the Atlantic Ocean. (c) Salinity at $\sigma_\theta = 25.0$ kg/m^3.

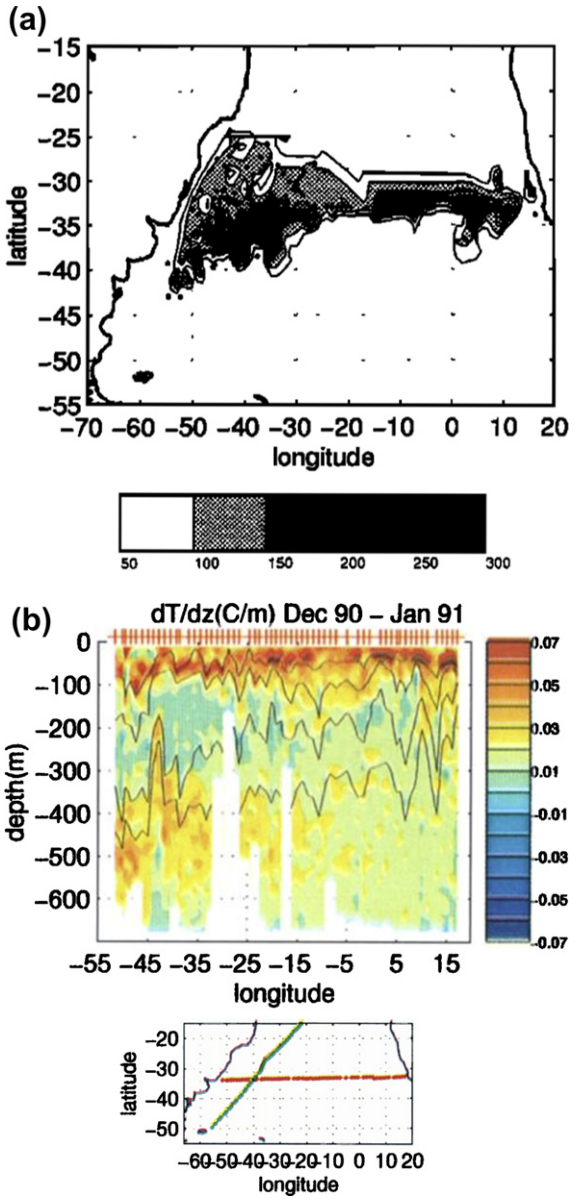

FIGURE S9.29 South Atlantic Subtropical Mode Water. (a) Thickness of the 14–16 °C layer. (b) Vertical temperature derivative along the east-west section in red on the map; 12, 14, 16, and 18 °C isotherms are indicated as black contours. *Source: From Provost et al. (1999).*

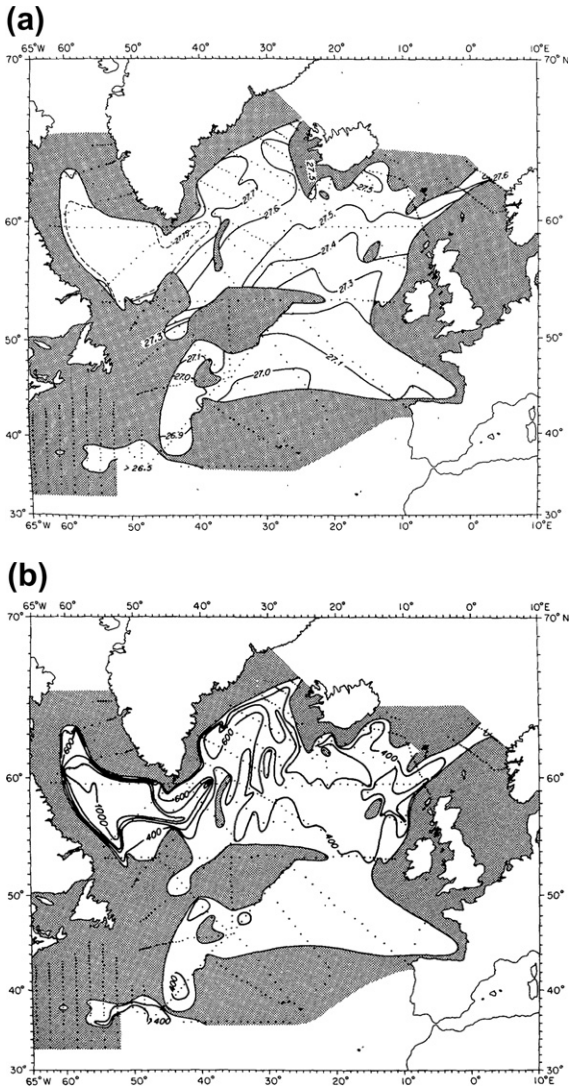

FIGURE S9.30 Subpolar Mode Water (SPMW). (a) Potential density (σ_θ) and (b) thickness (m) of the late winter mixed layer, shown only where the mixed layer is more than 200 m thick. This thick mixed layer is the SPMW. ©American Meteorological Society. Reprinted with permission. *Source: From McCartney and Talley (1982).*

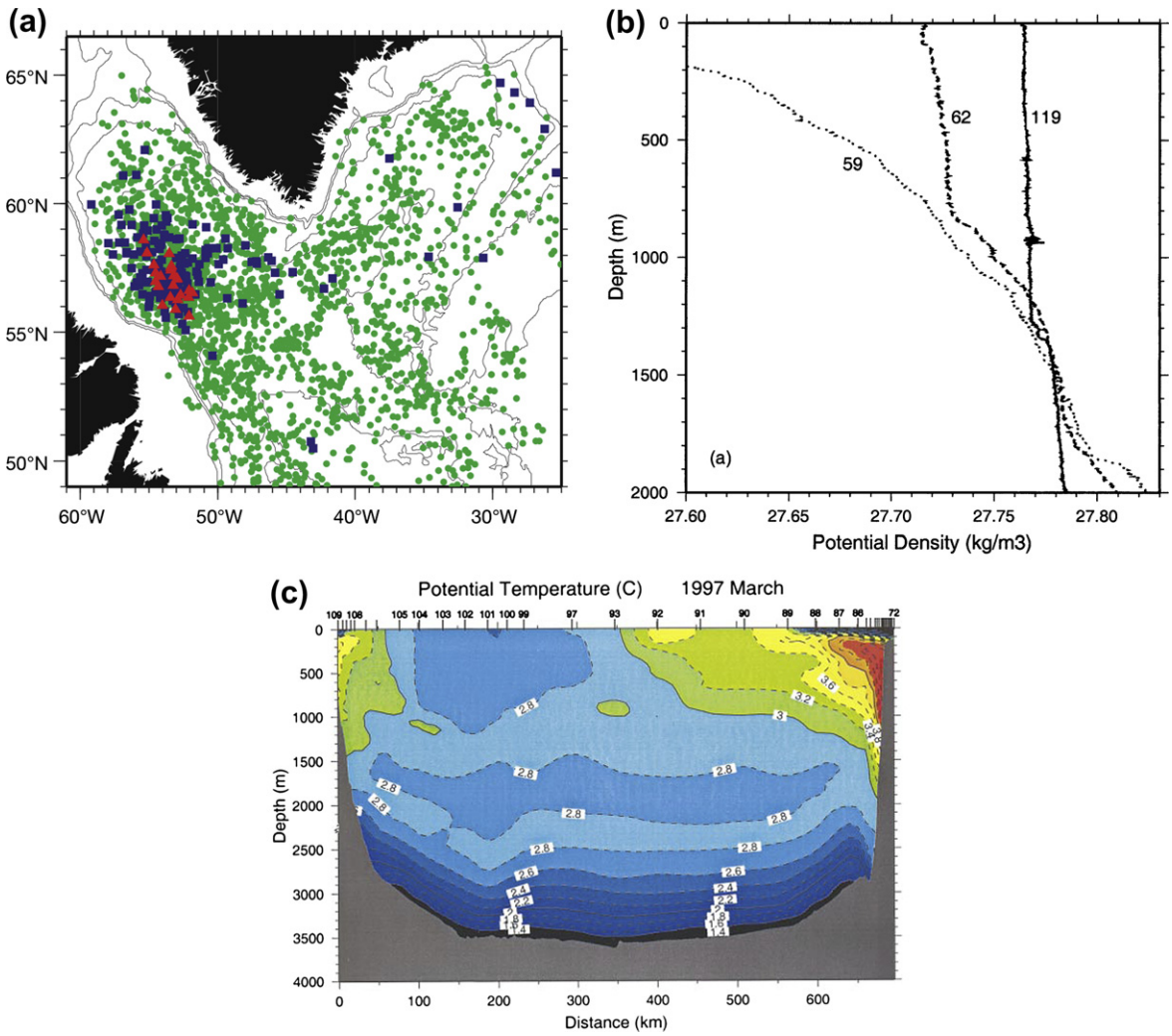

FIGURE S9.31 Labrador Sea Water. (a) Mixed layer depths in winter (1996–1998) from profiling floats. Red: >800 m. Blue: 400 to 800 m. Green: <400 m. *Source: From Lavender et al. (2000).* (b) Potential density profiles from a deep convection region in the Labrador Sea in late winter of 1997 ("119" in the deep convection patch, "62" in a western boundary convection regime, "59" typical of stratified water). (c) Vertical section through the Labrador Sea in late winter 1997 that includes deep convection stations. ©American Meteorological Society. Reprinted with permission. *Source: From Pickart, Torres, and Clarke (2002).*

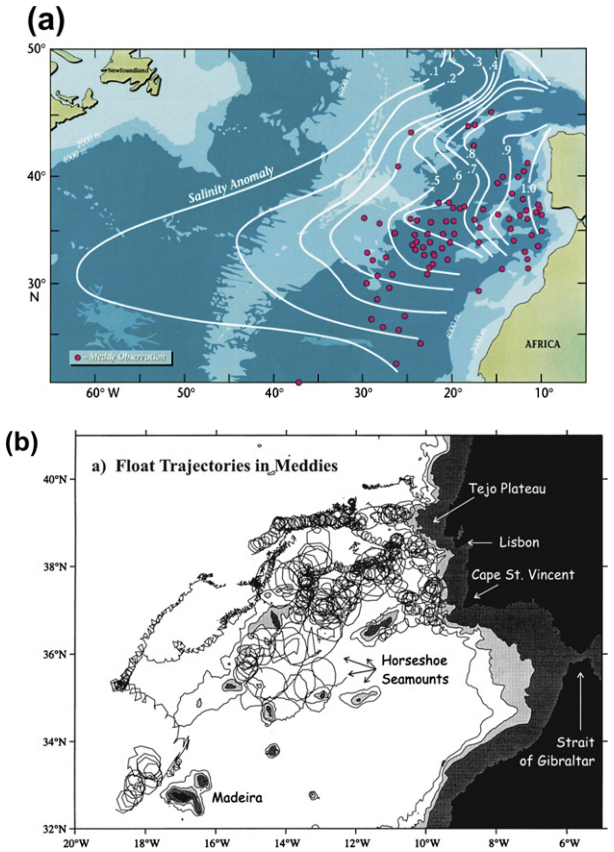

FIGURE S9.32 Meddies. (a) Occurrences in historical hydrographic data, superimposed on a map of salinity anomaly of Mediterranean Water near 1100 m depth. (b) Float trajectories in Meddies. *Source: From Richardson, Bower, and Zenk (2000).*

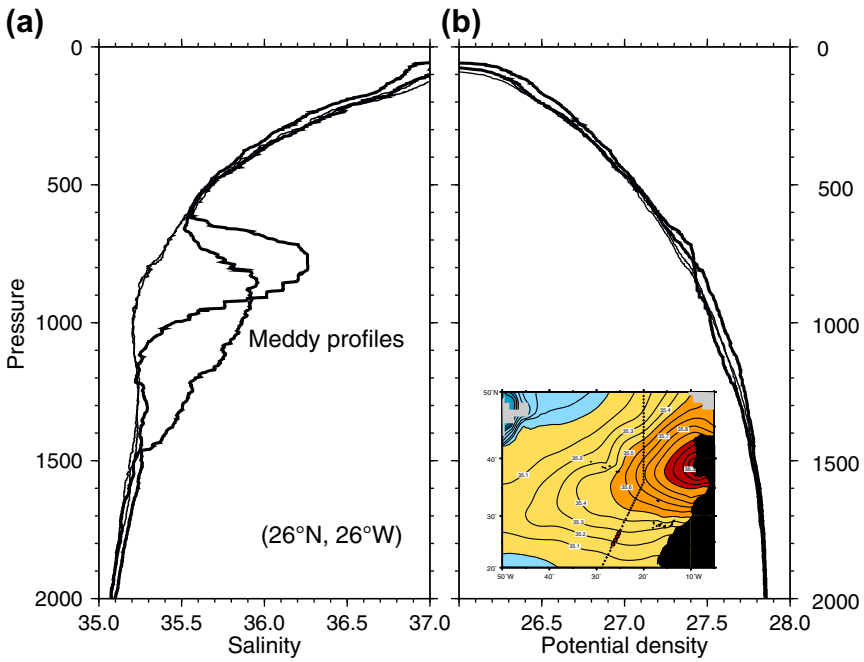

FIGURE S9.33 Meddy structure. (a) Salinity and (b) potential density through the only two Meddies found on a synoptic section in 1988, with adjacent profiles, at 26°N, 26°W (large dots on inset map). Inset map: salinity contoured at potential density referenced to 1000 dbar = 32.2 kg/m^3 (around σ_θ = 27.65 kg/m^3), with all stations from the 1988 section. *After Tsuchiya, Talley, and McCartney (1992).*

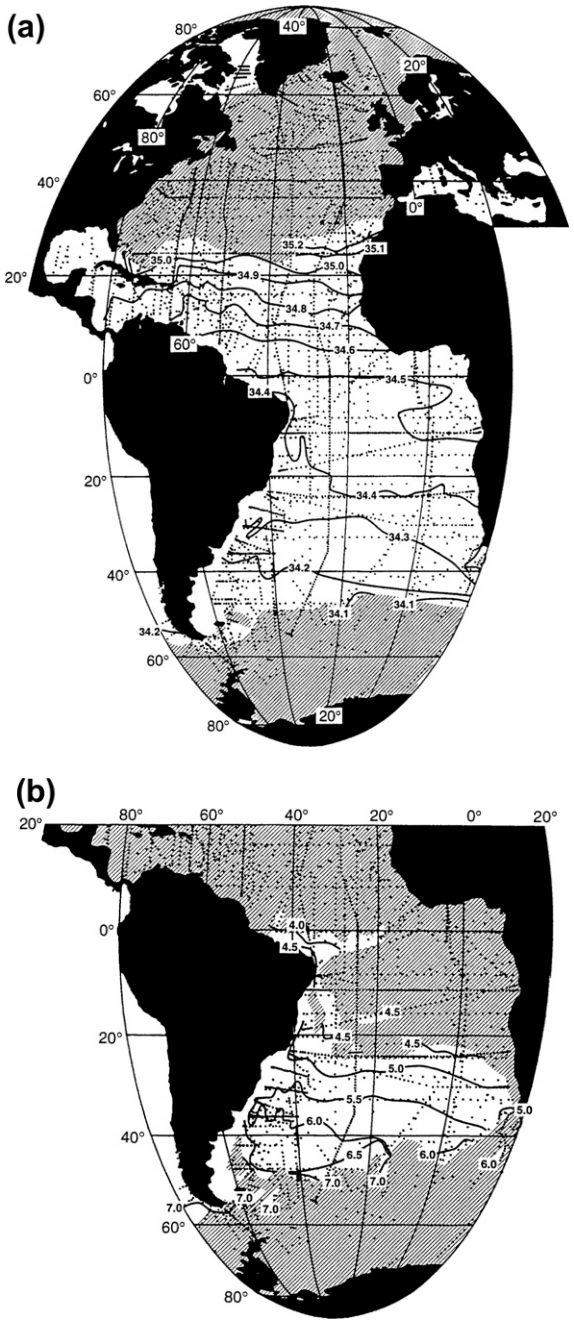

FIGURE S9.34 Antarctic Intermediate Water. (a) Salinity at the AAIW salinity minimum. (b) Oxygen (ml/L) at the AAIW oxygen maximum. *Source: From Talley (1996b).*

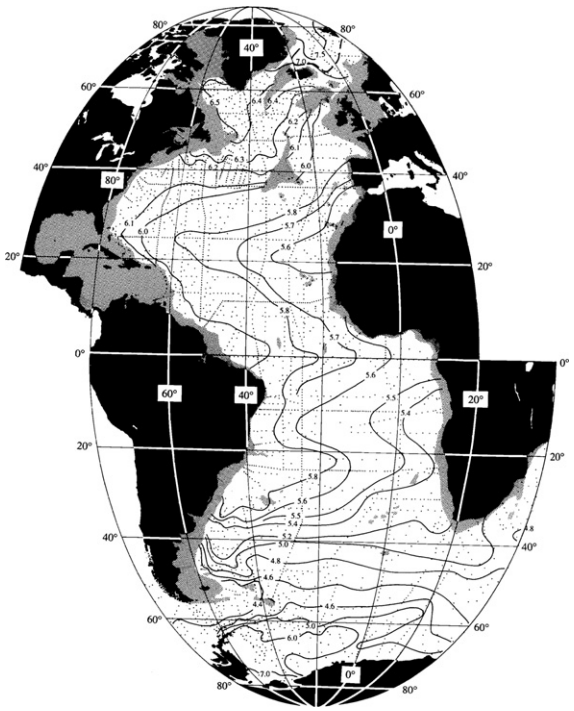

FIGURE S9.35 North Atlantic Deep Water and Circumpolar Deep Water. Oxygen (ml/L) on the isopycnal $s_3 = 41.44$ kg/m^3 (referenced to 3000 dbar), which lies at approximately 2500 m depth. *Source: From Reid (1994).*

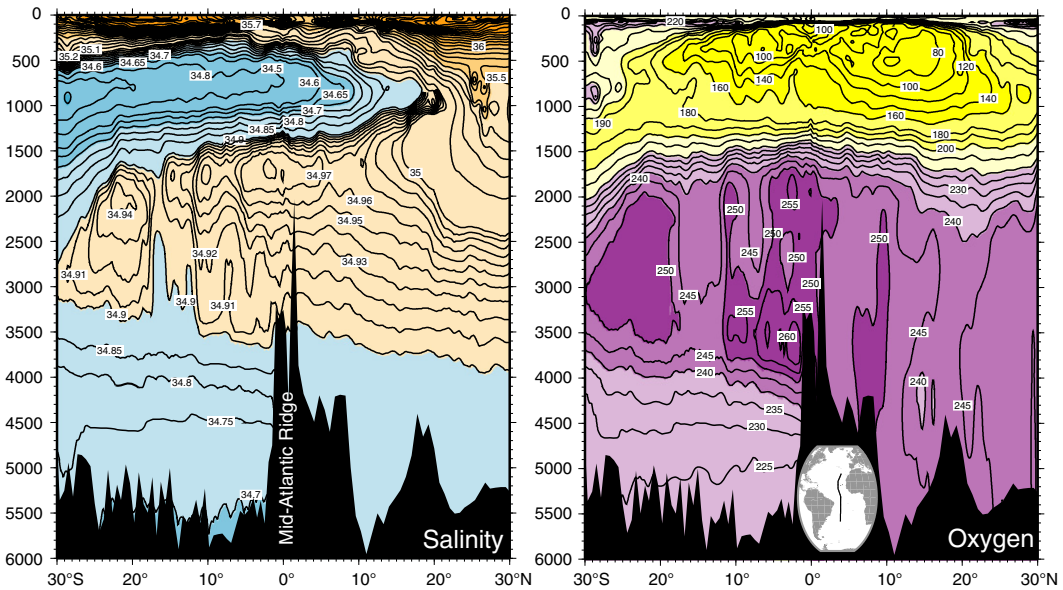

FIGURE S9.36 Upper, middle, and lower NADW in the tropical Atlantic. (a) Salinity and (b) oxygen (mmol/kg) along 25°W. Data were collected in 1988–1989. (World Ocean Circulation Experiment section A16).

TABLE S9.1 Major Upper Ocean Circulation Systems, Currents and Fronts of the Subtropical North Atlantic (Figures 9.1 and S9.1)*

Name	Description	Approximate Latitudes
Subtropical gyre	Anticyclonic gyre at mid-latitudes	10°–40°N
North Equatorial Current (NEC)	Westward flow of the subtropical gyre and northern tropical gyre	10–20°N
Gulf Stream System	Subtropical western boundary current complex	10–40 °N
Caribbean Current	Subtropical western boundary current portion within the Caribbean Sea	10–22°N
Yucatan Current	Subtropical western boundary current portion passing through Yucatan Channel	20–23°N
Loop Current (LC)	Subtropical western boundary current portion looping through the Gulf of Mexico	23–27°N
Antilles Current	Subtropical western boundary current portion east of the Antilles and Bahamas	18–28°N
Florida Current	Subtropical western boundary current portion through Florida Strait	12–28°N
Gulf Stream	Subtropical western boundary current north of Florida Strait and the separated extension of the subtropical western boundary current	28–35°N
Gulf Stream Extension	Eastern part of the separated Gulf Stream	35°N
Subtropical Countercurrent (STCC)	Eastward flow of the western subtropical gyre, south of the recirculation; continues into the Subtropical Front	22–25°N
Azores Current	Zonal eastward flow in the central and eastern subtropical gyre	33–36°N
Canary and Portugal Current Systems	Subtropical eastern boundary current system	23–46°N
Subtropical Frontal Zone	Zonal frontal band in the subtropical gyre; close to the maximum Ekman transport convergence	30–35°N

** Shading indicates the basic set.*

TABLE S9.2 Major Upper Ocean Circulation Systems, Currents and Fronts of the Subpolar North Atlantic (Figures 9.1 and S9.1)*

Name	Description	Approximate Location
Subpolar gyre	Cyclonic circulation at mid to high latitudes	45–65°N
North Atlantic Current (NAC)	Subtropical western boundary current and eastward flow of the subtropical and subpolar gyres; northeastward flow of subpolar gyre with three distinct branches	40–65°N
Labrador Current	Subpolar western boundary current	40–65°N
East Greenland Current (EGC)	Subpolar western boundary current on east coast of Greenland	North of 62°N
West Greenland Current (WGC)	Subpolar eastern boundary current on west coast of Greenland	60–65°N
Irminger Current	Northward flow along the western flank of the Reykjanes Ridge	55–64°N
Iceland Basin branch of the NAC	Northward flow of the NAC in the Iceland Basin	55–62°N
Rockall Trough branch of the NAC	North flow of the NAC in Rockall Trough	54–64°N
Iceland-Faroe Front (IFF)	Eastward flow along the Iceland-Faroe Ridge	62–66°N
North Iceland Current (NIC)	Eastward flow along north side of Iceland	66°N
Subarctic Frontal Zone	Frontal band separating subpolar and subtropical waters, within the North Atlantic Current	55–65°N

** Shading indicates the basic set.*

TABLE S9.3 Tropical and South Atlantic Circulation Systems and Currents*

Name	Description
North Equatorial Countercurrent (NECC)	Eastward flow at 5–10°N
North Brazil Current (NBC)	Northward-flowing low latitude western boundary current
South Equatorial Current (SEC)	Westward flow in equatorial region ("North" and "Central" SEC) and on the equatorial side of the South Atlantic's subtropical gyre ("South" SEC)
Equatorial Undercurrent (EUC)	Eastward subsurface flow along equator
Equatorial Intermediate Current (EIC)	Westward flow beneath the Equatorial Undercurrent along the equator
South Equatorial Countercurrent (SECC)	Eastward flow at 7–9°S
Guinea Current	Eastward flow along the coast of Africa north of the equator
Guinea Dome	Upwelling region with cyclonic circulation in the eastern tropical North Atlantic
Angola Current	Southward tropical eastern boundary current between the equator and 16°S
Angola Dome	Upwelling region with cyclonic circulation in the eastern tropical South Atlantic
Subtropical gyre	Anticyclonic gyre at mid-latitudes
Brazil Current (BC)	Western boundary current of the subtropical gyre along the coast of Australia
South Atlantic Current (or Westwind Drift; SAC)	Eastward flow of the subtropical gyre
Benguela Current System (BCS)	Eastern boundary current system for the subtropical gyre; 34–14°S
Agulhas Retroflection	Retroflection of the Indian Ocean's Agulhas Current
Subantarctic Front (SAF)	Eastward flow in the northernmost front of the Antarctic Circumpolar Current
Malvinas (Falkland) Current	Western boundary current that is a northward loop of the Subantarctic Front
Deep Western Boundary Current (DWBC)	Deep boundary currents in the NADW and AABW layers

** Shading indicates the basic set.*

TABLE S9.4 Principal Atlantic Ocean Water Masses*

Water Mass	Characteristic in the Vertical	Layer	Formation Process
North Atlantic Central Water (NACW)	Subtropical thermocline waters	Upper 0–1000 m	Subduction
South Atlantic Central Water (SACW)	Subtropical thermocline waters	Upper 0–1000 m	Subduction
North Atlantic Subtropical Underwater (NASTUW)	Subtropical/tropical salinity maximum	Upper 50–100 m	Subduction of high salinity subtropical surface waters
South Atlantic Subtropical Underwater (SASTUW)	Subtropical/tropical salinity maximum	Upper 50–100 m	Subduction of high salinity subtropical surface waters
North Atlantic Subtropical Mode Water or Eighteen Degree Water (EDW)	Subtropical stability (potential vorticity) minimum	Upper 0–400 m	Subduction of thick, convective winter mixed layer
Subpolar Mode Water (SPMW)	North Atlantic stability (potential vorticity) minimum	Upper 0–700 m	Thick, convective winter mixed layer
South Atlantic Subtropical Mode Water (SASTMW)	Subtropical stability (potential vorticity) minimum	Upper 0–300 m	Subduction of thick, convective winter mixed layer
Subantarctic Mode Water (SAMW)	Potential vorticity minimum and oxygen maximum in subtropical South Atlantic	Upper 0–600 m	Subducted thick winter mixed layers north of Subantarctic Front
Labrador Sea Water (LSW)	Salinity and potential vorticity minimum in subpolar and western North Atlantic	Intermediate 200–2000 m	Deep convection in the Labrador Sea
Mediterranean Water (MW; or Mediterranean Overflow Water or Mediterranean Outflow Water, MOW)	Salinity maximum in North Atlantic subtropical gyre and tropics	Intermediate 700–1700 m	Deep convection in the Mediterranean Sea, overflow through Strait of Gibraltar
Antarctic Intermediate Water (AAIW)	Salinity minimum in subtropical S. Atlantic and tropical Atlantic	Intermediate 500–1200 m	Advection of fresh subantarctic surface water
Nordic Seas Overflow Water (NSOW)	Oxygen maximum in the northern North Atlantic	Deep 600–4500 m	Deep convection in the Greenland Sea, overflow into the North Atlantic
Denmark Strait Overflow Water (DSOW)	Oxygen maximum in the deep northern North Atlantic	Deep 600–4500 m	Nordic Seas overflow through Denmark Strait
Iceland Scotland Overflow Water (ISOW)	Salinity maximum in the deep northern North Atlantic	Deep 2500–3500 m	Nordic Seas overflow across the Iceland-Scotland ridge

(*Continued*)

TABLE S9.4 Principal Atlantic Ocean Water Masses* —Cont'd

Water Mass	Characteristic in the Vertical	Layer	Formation Process
Northeast Atlantic Deep Water (NEADW)	Oxygen minimum, salinity maximum in deep eastern North Atlantic	Deep 2500–4500 m	Mixture of all NADW sources and AABW
North Atlantic Deep Water (NADW)	Oxygen minimum, nutrient maximum, salinity maximum	Deep 1000–4500 m	Mixing and aging of deep waters
Upper Circumpolar Deep Water (UCDW)	Low oxygen	Deep ~1000– 3000 m	Mixture of IDW, PDW, and deep waters in the Southern Ocean
Weddell Sea Deep Water (WSDW)	Cold, dense	Near surface to bottom	Brine rejection and convection in the Southern Ocean
Antarctic Bottom Water (AABW)	Deep salinity and oxygen maxima, nutrient minima	Bottom 3000 m to bottom	Brine rejection in the Southern Ocean, mixed with NADW, PDW and IDW

** Shading indicates the basic set.*

References

Bane, J.M., 1994. The Gulf Stream System: An observational perspective. Chapter 6. In: Majumdar, S.K., Miller, E.W., Forbes, G.S., Schmalz, R.F., Panah, A.A. (Eds.), The Oceans: Physical-Chemical Dynamics and Human Impact. The Pennsylvania Academy of Science, pp. 99–107.

Baringer, M., Larsen, J., 2001. Sixteen years of Florida Current transport at 27°N. Geophys. Res. Lett. 28, 3179–3182.

Beal, L.M., Hummon, J.M., Williams, E., Brown, O.B., Baringer, W., Kearns, E.J., 2008. Five years of Florida Current structure and transport from the Royal Caribbean Cruise Ship Explorer of the Seas. J. Geophys. Res. 113 C06001. doi:10.1029/2007JC004154.

Biastoch, A., Böning, C.W., Lutjeharms, J.R.E., 2008. Agulhas leakage dynamics affects decadal variability in the Atlantic overturning circulation. Nature 456, 489–492.

Boebel, O., Davis, R.E., Ollitrault, M., Peterson, R.G., Richardson, P.L., Schmid, C., Zenk, W., 1999. The intermediate depth circulation of the western. South Atlantic. Geophys. Res. Lett. 26, 21. doi:10.1029/1999GL002355.

Bower, A.S., LeCann, B., Rossby, T., Zenk, W., Gould, J., Speer, K., Richardson, P.L., Prater, M.D., Zhang, H.-M., 2002. Directly measured mid-depth circulation in the northeastern North Atlantic Ocean. Nature 410, 603–607.

Bryden, H.L., Longworth, H.R., Cunningham, S.A., 2005b. Slowing of the Atlantic meridional overturning circulation at 26.5°N. Nature 438, 655–657.

Candela, J., Tanahara, S., Crepon, M., Barnier, B., Sheinbaum, J., 2003. Yucatan Channel flow: Observations versus CLIPPER ATL6 and MERCATOR PAM models. J. Geophys. Res. 108, 3385. doi:10.1029/2003JC00196.

Dengler, M., Schott, F.A., Eden, C., Brandt, P., Fischer, J., Zantopp, R.J., 2004. Break-up of the Atlantic deep western boundary current into eddies at 8°S. Nature 432, 1018–1020.

Dickson, R., Brown, J., 1994. The production of North Atlantic Deep Water: Sources, rates, and pathways. J. Geophys. Res. 99, 12319–12341.

Fratantoni, D.M., 2001. North Atlantic surface circulation during the 1990s observed with satellite-tracked drifters. J. Geophys. Res. 106, 22067–22093.

Ganachaud, A., 2003. Large-scale mass transports, water mass formation, and diffusivities estimated from World Ocean Circulation Experiment (WOCE) hydrographic data. J. Geophys. Res. 108 (C7), 3213. doi: 10.1029/2002JC002565.

Hogg, N.G., 1983. A note on the deep circulation of the western North Atlantic: Its nature and causes. Deep-Sea Res. 30, 945–961.

Hogg, N.G., Owens, W.B., 1999. Direct measurement of the deep circulation within the Brazil Basin. Deep-Sea Res. II 46, 335–353.

Hogg, N.G., Siedler, G., Zenk, W., 1999. Circulation and variability at the southern boundary of the Brazil Basin. J. Phys. Oceanogr 29, 145–157.

Johns, W.E., Townsend, T.L., Fratantoni, D.M., Wilson, W.D., 2002. On the Atlantic inflow to the Caribbean Sea. Deep-Sea Res. I 49, 211–243.

Juliano, M.F., Alvés, M.L.G.R., 2007. The Subtropical Front/Current systems of Azores and St. Helena. J. Phys. Oceanogr 37, 2573–2598.

Kalnay, E., Kanamitsu, M., Kistler, R., Collins, W., Deaven, D., Gandin, L., et al., 1996. The NCEP-NCAR 40-year reanalysis project. B. Am. Meteorol. Soc. 77, 437–471.

Large, W.G., Yeager, S.G., 2009. The global climatology of an interannually varying air-sea flux data set. Clim. Dynam 33, 341–364.

Lavender, K.L., Davis, R.E., Owens, W.B., 2000. Mid-depth recirculation observed in the interior Labrador and Irminger seas by direct velocity measurements. Nature 407, 66–69.

Lentini, C.A.D., Goni, G.J., Olson, D.B., 2006. Investigation of Brazil Current rings in the confluence region. J. Geophys. Res, 111. C06013. doi:10.1029/2005JC002988.

McCartney, M.S., Talley, L.D., 1982. The Subpolar Mode Water of the North Atlantic Ocean. J. Phys. Oceanogr 12, 1169–1188.

Niiler, P.P., Maximenko, N.A., McWilliams, J.C., 2003. Dynamically balanced absolute sea level of the global ocean derived from near-surface velocity observations. Geophys. Res. Lett. 30, 22. doi:10.1029/2003GL018628.

Olson, D., Schmitt, R., Kennelly, M., Joyce, T., 1985. A two-layer diagnostic model of the long-term physical evolution of warm-core ring 82B. J. Geophys. Res. 90, 8813–8822.

Owens, W.B., 1991. A statistical description of the mean circulation and eddy variability in the northwestern Atlantic using SOFAR floats. Progr. Oceanogr 28, 257–303.

Parker, C.E., 1971. Gulf Stream rings in the Sargasso Sea. Deep-Sea Res. 18, 981–993.

Peeters, F.J.C., Acheson, R., Brummer, G.-J.A., de Ruijter, W.P.M., Schneider, R.R., Ganssen, G.M., Ufkes, E., Kroon, D., 2004. Vigorous exchange between the Indian and Atlantic oceans at the end of the past five glacial periods. Nature 430, 661–665.

Peterson, R.G., 1992. The boundary currents in the western Argentine Basin. Deep-Sea Res. 39, 623–644.

Pickart, R.S., McKee, T.K., Torres, D.J., Harrington, S.A., 1999. Mean structure and interannual variability of the slopewater system south of Newfoundland. J. Phys. Oceanogr 29, 2541–2558.

Pickart, R.S., Torres, D.J., Clarke, R.A., 2002. Hydrography of the Labrador Sea during active convection. J. Phys. Oceanogr 32, 428–457.

Provost, C., Escoffier, C., Maamaatuaiahutapu, K., Kartavtseff, A., Garçon, V., 1999. Subtropical mode waters in the South Atlantic Ocean. J. Geophys. Res. 104, 21033–21049.

Reid, J.L., 1994. On the total geostrophic circulation of the North Atlantic Ocean: Flow patterns, tracers and transports. Progr. Oceanogr 33, 1–92.

Richardson, P.L., 2005. Caribbean Current and eddies as observed by surface drifters. Deep-Sea Res. II 52, 429–463.

Richardson, P.L., Bower, A.S., Zenk, W., 2000. A census of Meddies tracked by floats. Progr. Oceanogr 45, 209–250.

Roemmich, D.L., 1983. Optimal estimation of hydrographic station data and derived fields. J. Phys. Oceanogr 13, 1544–1549.

Rossby, T., 1999. On gyre interactions. Deep-Sea Res. II 46, 139–164.

Schmitz, W.J., 1996b. On the World Ocean Circulation: Volume I: Some global features/North Atlantic circulation. Woods Hole Oceanographic Institution Technical Report, WHOI-96-03. Woods Hole, MA, 141 pp.

Schott, F., Zantopp, R., Stramma, L., Dengler, M., Fischer, J., Wibaux, M., 2004. Circulation and deep water export at the western exit of the subpolar North Atlantic. J. Phys. Oceanogr 34, 817–843.

Talley, L.D., 1996b. North Atlantic circulation and variability, reviewed for the CNLS conference. Physica D 98, 625–646.

Tsuchiya, M., Talley, L.D., McCartney, M.S., 1992. An eastern Atlantic section from Iceland southward across the equator. Deep-Sea Res. 39, 1885–1917.

van Aken, H.M., van Veldhoven, A.K., Veth, C., de Ruijter, W.P.M., van Leeuwen, P.J., Drijfhout, S.S., Whittle, C.P., Rouault, M., 2003. Observations of a young Agulhas ring, Astrid, during MARE in March 2000. Deep-Sea Res. II 50, 167–195.

Zemba, J.C., 1991. The structure and transport of the Brazil Current between 27° and 36° South. Ph.D. Thesis. Massachusetts Institute of Technology and Woods Hole Oceanographic Institution, 160 pp.